

Modeling and analysis of spiral actuators by exact geometry piezoelectric solid-shell elements

GM Kulikov¹ , SV Plotnikova¹ and E Carrera²

Journal of Intelligent Material Systems and Structures

2020, Vol. 31(1) 53–70

© The Author(s) 2019

Article reuse guidelines:

sagepub.com/journals-permissions

DOI: 10.1177/1045389X19880014

journals.sagepub.com/home/jim



Abstract

An exact geometry four-node piezoelectric solid-shell element through the sampling surfaces formulation is proposed. The sampling surfaces formulation is based on choosing inside the shell $N - 2$ sampling surfaces parallel to the middle surface and located at Chebyshev polynomial nodes to introduce the displacements and electric potentials of these surfaces as fundamental shell unknowns. The bottom and top surfaces are also included into a set of sampling surfaces. Such choice of unknowns with the use of Lagrange polynomials of degree $N - 1$ in the through-the-thickness interpolations of displacements, strains, electric potential, and electric field yields a robust piezoelectric shell formulation. To implement efficient analytical integration throughout the solid-shell element, the extended assumed natural strain method is employed. The developed hybrid-mixed four-node piezoelectric solid-shell element is based on the Hu-Washizu variational principle and shows the excellent performance for coarse mesh configurations. It can be useful for the 3D stress analysis of piezoelectric shells with variable curvatures, in particular for the modeling and analysis of spiral actuators.

Keywords

Spiral piezoelectric actuator, exact geometry solid-shell element, hybrid-mixed method, higher-order SaS formulation

1. Introduction

Nowadays, the piezoelectric ceramics are widely used as actuators in transducers and advanced electronic systems. An interesting application of the piezoelectric ceramics is a spiral actuator with the compact geometry designed by Mohammadi et al. (1999), Allahverdi et al. (2001), Li and Gianchandani (2006), and Lee et al. (2008) in order to enlarge the field-induced displacement in a tangential direction due to the nonuniform stress distribution arisen under the applied voltage. In the case of applying the electric field to a spiral actuator in the poling direction across its thickness, the spiral tip moves in tangential and radial directions. As it turned out, the tangential displacement is more than 12 times greater than the transverse displacement of the piezoelectric strip of the same length under the same voltage (Allahverdi et al., 2001). This problem attracted many researchers (Lee et al., 2008; Li and Gianchandani, 2006; Zouari et al., 2009) who modeled the spiral actuator with solid elements available in the literature. However, the modeling of spiral actuators using solid elements is too expensive (Zouari et al., 2009) because very many elements should be used to describe the geometry of the spiral properly.

More reliable results can be obtained through the isoparametric six-parameter piezoelectric solid-shell elements (Klinkel and Wagner, 2006, 2008; Lee et al., 2003; Lentzen, 2009; Sze et al., 2000; Sze and Yao, 2000; Tan and Vu-Quoc, 2005; Yao and Sze, 2009; Zheng et al., 2004). These elements are defined by two layers of nodes on outer surfaces of the shell with three displacement degrees of freedom (DOFs) and one electric potential DOF per node. However, the six-parameter solid-shell element formulation based on the complete constitutive equations of piezoelectricity has a deficiency because of Poisson thickness locking. This is because the linear displacement field in the thickness direction leads to a constant transverse normal strain, which causes artificial stiffening of the shell element for nonvanishing Poisson's ratios. To avoid Poisson

¹Laboratory of Intelligent Materials and Structures, Tambov State Technical University, Tambov, Russia

²Department of Aeronautics and Aerospace Engineering, Politecnico di Torino, Turin, Italy

Corresponding author:

GM Kulikov, Laboratory of Intelligent Materials and Structures, Tambov State Technical University, Sovetskaya 106, Tambov 392000, Russia.
Email: gmkulikov@mail.ru

thickness locking, the 3D constitutive equations should be modified using the generalized plane stress conditions (Lee et al., 2003). The hybrid stress method (Sze et al., 2000; Sze and Yao, 2000; Yao and Sze, 2009), in which the transverse normal stress is assumed to be constant through the thickness, and the most popular enhanced assumed strain method (Klinkel and Wagner, 2006, 2008; Lentzen, 2009; Tan and Vu-Quoc, 2005; Zheng et al., 2004), in which the transverse normal strain is enriched in the thickness direction by a linear term, can be also applied. Still, the isoparametric solid-shell element formulation is computationally inefficient because stresses and strains are analyzed in the global and local orthogonal Cartesian coordinate systems, although the normalized element coordinates represent already convected curvilinear coordinates. The isoparametric solid elements can be also utilized efficiently for the analysis of piezoelectric structures (see, for example, Kpeky et al., 2018; Yi et al., 2000; Zouari et al., 2012, 2015).

An alternative way is to develop the exact geometry or geometrically exact (GeX) six-parameter piezoelectric solid-shell element based on the direct use of curvilinear coordinates of the middle surface (Kulikov and Plotnikova, 2008). The term GeX means that the parametrization of the middle surface is known and, therefore, the coefficients of the first and second fundamental forms and the Christoffel symbols are taken exactly at element nodes. In contrast to the six-parameter solid-shell element (Kulikov and Plotnikova, 2008), the GeX seven-parameter solid-shell elements (Kulikov and Plotnikova, 2010, 2011a) are based on the choice of six displacements and two electric potentials of outer surfaces and the transverse displacement of the middle surface. The seven-parameter shell formulation is optimal concerning the number of DOFs and allows the use of complete constitutive equations of piezoelectricity. The more general GeX nine-parameter solid-shell elements, in which nine displacements and three electric potentials of outer and middle surfaces are introduced as basic shell unknowns, have been developed by Kulikov and Plotnikova (2011b, 2015). In this model, the Lagrange polynomials of the second degree are utilized to describe the approximations of displacements, strains, electric potential, and electric field through the thickness that makes possible to derive the strain-displacement equations, which exactly represent all rigid body motions of the shell in curvilinear coordinates of the middle surface. This fact is of great importance since one may read in paper (Buechter and Ramm, 1992) that “shell theory is an absolute academic exercise” due to “the difficulties of representing the rigid body modes in shell finite element formulations.”

It should be noted that the aforementioned isoparametric and GeX piezoelectric solid-shell elements (Klinkel and Wagner, 2006, 2008; Kulikov and

Plotnikova, 2008, 2010, 20011a, 2011b, 2015; Lee et al., 2003; Lentzen, 2009; Sze et al., 2000; Sze and Yao, 2000; Tan and Vu-Quoc, 2005; Yao and Sze, 2009; Zheng et al., 2004) cannot describe properly the transverse components of the stress tensor and the electric displacement vector. To solve the problem, the higher-order models should be invoked (Carrera et al., 2011; Vidal et al., 2016). The robust GeX higher-order piezoelectric solid-shell elements have been developed by Carrera et al. (2011, 2014) through the Carrera’s unified formulation (Carrera, 2003). In contributions (Carrera et al., 2018; Carrera and Valvano, 2017; Cinefra et al., 2015), the shear and membrane locking phenomena are prevented by using the mixed interpolation of tensorial components (MITC) technique (Bathe and Dvorkin, 1986). These higher-order solid-shell elements were applied efficiently to the 3D stress analysis of piezoelectric plates and cylindrical shells. As it turned out, the evaluation of the transverse normal stress and electric displacement is not a simple problem because using even the fourth-order Legendre polynomials in the through-thickness approximations of displacements does not provide fulfilling the boundary conditions for these components on outer surfaces (Cinefra et al., 2015).

The objective of this work is to overcome the above difficulties and develop the higher-order piezoelectric solid-shell element that permits the evaluation of all stress and electric displacement components for the shell structures of complicated geometry with applications to the spiral actuators. For this purpose, the GeX four-node piezoelectric solid-shell element through the sampling surfaces (SaS) formulation (Kulikov and Plotnikova, 2013) is proposed. The SaS formulation is based on choosing throughout the shell N not equally spaced surfaces parallel to the middle surface to introduce the displacements and electric potentials of these surfaces as fundamental shell unknowns, where $N \geq 3$. Such choice of unknowns with the use of Lagrange polynomials of degree $N - 1$ in the assumed through-thickness distributions of displacements, strains, electric potential and electric field yields a very compact piezoelectric shell formulation. Recently, the SaS formulation has been employed to analyze analytically and numerically the electroelastic and thermoelectroelastic response of laminated and functionally graded piezoelectric plates and cylindrical shells (Kulikov et al., 2015, 2018; Kulikov and Plotnikova, 2017a, 2017b).

The SaS method can be traced to contributions (Kulikov, 2001; Kulikov and Carrera, 2008; Kulikov and Plotnikova, 2011c) in which the equispaced SaS are utilized. The more general approach with the SaS located at Chebyshev polynomial nodes, that is, the roots of the Chebyshev polynomial (Bakhvalov, 1977) has been proposed by Kulikov and Plotnikova (2013) since the SaS formulation with equally spaced SaS does not work properly with the higher-order Lagrange

interpolation. The use of Chebyshev polynomial nodes improves the behavior of high-degree Lagrange polynomials because it allows one to minimize uniformly the error due to the Lagrange interpolation.

In the present article, the GeX hybrid-mixed four-node piezoelectric solid-shell element is developed with the SaS located at Chebyshev nodes or Chebyshev-Gauss-Lobatto points. To prevent shear and membrane locking, the assumed interpolations of displacement-independent strains and stresses are employed. For this purpose, the Hu-Washizu variational principle is invoked. This approach has some computational advantages compared with conventional isoparametric hybrid-mixed piezoelectric solid-shell element formulations. This is because the element matrices are evaluated with no expensive numerical matrix inversion. It is impossible in the framework of the isoparametric hybrid-mixed shell elements (Hoa and Feng, 1998). The important feature of the GeX solid-shell element is the use of effective analytical integration throughout the element by an extended assumed natural strain (ANS) method (Kulikov and Plotnikova, 2015).

The proposed GeX/SaS piezoelectric solid-shell element formulation is characterized by the following features and new developments:

- Here, we do not exclude the electric displacement vector from the SaS solid-shell element formulation using the constitutive equations as in Kulikov et al. (2018) because it is more efficient to utilize the SaS approximation for the electric displacement components (equation 8). This novelty simplifies the implementation of the hybrid-mixed method and allows the presentation of governing equations in terms of only SaS variables that provides superior performance in the case of coarse meshes.
- To show that the proposed GeX piezoelectric solid-shell element is free of spurious zero-energy modes, we consider the eigenvalues problem for a piezoelectric rectangular parallelepiped. As it turned out, there exist exactly seven zero-energy modes, namely six modes related to the rigid body motions and one to the short circuit.
- The coupled electromechanical model (Kulikov et al., 2018) is extended to the 3D stress analysis of the piezoelectric shells of complicated geometry with particular attention to the spiral actuators whose middle surface can be described by orthogonal curvilinear coordinates.

2. SaS formulation for piezoelectric shell

Consider a shell of the thickness h . The middle surface Ω is described by orthogonal curvilinear coordinates θ_1 and θ_2 , which are referred to the lines of principal

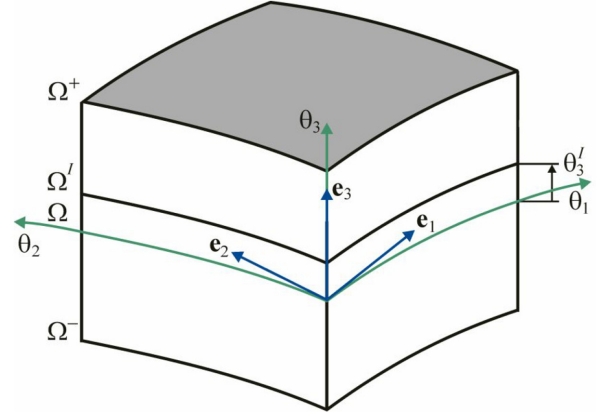


Figure 1. Geometry of the piezoelectric shell.

curvatures of its surface. The coordinate θ_3 is oriented along the unit vector \mathbf{e}_3 normal to the middle surface. Introduce the following notations: \mathbf{e}_α are the orthonormal base vectors of the middle surface; $c_\alpha = 1 + k_\alpha \theta_3$ are the components of the shifter tensor; k_α are the principal curvatures of the middle surface; $c_\alpha^I = c_\alpha(\theta_3^I) = 1 + k_\alpha \theta_3^I$ are the components of the shifter tensor at SaS Ω^I depicted in Figure 1; θ_3^I are the transverse coordinates of SaS defined as

$$\begin{aligned} \theta_3^1 &= -\frac{h}{2}, & \theta_3^N &= \frac{h}{2} \\ \theta_3^n &= -\frac{h}{2} \cos\left(\pi \frac{2n-3}{2(N-2)}\right), & n &= 2, \dots, N-1 \end{aligned} \quad (1)$$

where N is the number of SaS. Here and in the following developments, the indices I, J, K identify the belonging of any quantity to the SaS and run from 1 to N ; Latin indices i, j, k, l range from 1 to 3; Greek indices α, β range from 1 to 2.

It is worth noting that the inner SaS are located at the roots of the Chebyshev polynomial of degree $N-2$ (Bakhvalov, 1977). However, the SaS located at Chebyshev-Gauss-Lobatto points can be also utilized

$$\theta_3^I = -\frac{h}{2} \cos\left(\pi \frac{I-1}{N-1}\right) \quad (2)$$

The through-thickness SaS approximations (Kulikov and Plotnikova, 2013) can be written as

$$u_i = \sum_I L^I u_i^I, \quad u_i^I = u_i(\theta_3^I) \quad (3)$$

$$\varepsilon_{ij} = \sum_I L^I \varepsilon_{ij}^I, \quad \varepsilon_{ij}^I = \varepsilon_{ij}(\theta_3^I) \quad (4)$$

$$\sigma_{ij} = \sum_I L^I \sigma_{ij}^I, \quad \sigma_{ij}^I = \sigma_{ij}(\theta_3^I) \quad (5)$$

$$\phi = \sum_I L^I \phi^I, \quad \phi^I = \phi(\theta_3^I) \quad (6)$$

$$E_i = \sum_I L^I E_i^I, \quad E_i^I = E_i(\theta_3^I) \quad (7)$$

$$D_i = \sum_I L^I D_i^I, \quad D_i^I = D_i(\theta_3^I) \quad (8)$$

where u_i , ε_{ij} , σ_{ij} , ϕ , E_i , and D_i are the displacements, strains, stresses, electric potential, electric field, and electric displacement; $u_i^I(\theta_1, \theta_2)$, $\varepsilon_{ij}^I(\theta_1, \theta_2)$, $\sigma_{ij}^I(\theta_1, \theta_2)$, $\phi^I(\theta_1, \theta_2)$, $E_i^I(\theta_1, \theta_2)$, and $D_i^I(\theta_1, \theta_2)$ are the displacements, strains, stresses, electric potential, electric field, and electric displacement of SaS Ω^I ; $L^I(\theta_3)$ are the Lagrange basis polynomials of degree $N-1$ defined as

$$L^I = \prod_{J \neq I} \frac{\theta_3 - \theta_3^J}{\theta_3^I - \theta_3^J} \quad (9)$$

In an orthonormal basis \mathbf{e}_i , the relations between SaS strains and SaS displacements (Kulikov and Plotnikova, 2013) are expressed as

$$2\varepsilon_{\alpha\beta}^I = \frac{1}{c_\beta^I} \lambda_{\alpha\beta}^I + \frac{1}{c_\alpha^I} \lambda_{\beta\alpha}^I \quad (10)$$

$$2\varepsilon_{\alpha 3}^I = \beta_\alpha^I + \frac{1}{c_\alpha^I} \lambda_{3\alpha}^I, \quad \varepsilon_{33}^I = \beta_3^I$$

where $\lambda_{\alpha\beta}^I$ are the strain parameters of SaS; $\beta_i^I = u_{i,3}(\theta_3^I)$ are the values of displacement derivatives with respect to the thickness coordinate on SaS given by

$$\lambda_{\alpha\alpha}^I = \frac{1}{A_\alpha} u_{\alpha,\alpha}^I + B_\alpha u_\beta^I + k_\alpha u_3^I \quad (11)$$

$$\lambda_{\beta\alpha}^I = \frac{1}{A_\alpha} u_{\beta,\alpha}^I - B_\alpha u_\alpha^I \text{ for } \beta \neq \alpha$$

$$\lambda_{3\alpha}^I = \frac{1}{A_\alpha} u_{3,\alpha}^I - k_\alpha u_\alpha^I, \quad B_\alpha = \frac{1}{A_\alpha A_\beta} A_{\alpha,\beta} \text{ for } \beta \neq \alpha$$

$$\beta_i^I = \sum_J M^J(\theta_3^I) u_i^J$$

where A_α are the coefficients of the first fundamental form; the symbol $(\dots)_i$ stands for the partial derivatives with respect to coordinates θ_i ; $M^J = L_{,3}^J$ are the polynomials of degree $N-2$ whose values on SaS $M^J(\theta_3^I)$ are calculated according to Kulikov and Plotnikova (2013).

In an orthonormal basis \mathbf{e}_i , the relations between the electric field and electric potentials of SaS (Kulikov and Plotnikova, 2013) are written as

$$E_\alpha^I = -\frac{1}{A_\alpha c_\alpha^I} \phi_{,\alpha}^I, \quad E_3^I = -\sum_J M^J(\theta_3^I) \phi^J \quad (12)$$

3. Electroelastic energy of piezoelectric shell

The constitutive equations in terms of SaS variables (Kulikov and Plotnikova, 2013) are expressed as

$$\boldsymbol{\sigma}^I = \mathbf{C}\boldsymbol{\varepsilon}^I - \mathbf{e}^T \mathbf{E}^I \quad (13)$$

$$\mathbf{D}^I = \mathbf{e}\boldsymbol{\varepsilon}^I + \boldsymbol{\varepsilon} \mathbf{E}^I \quad (14)$$

where

$$\begin{aligned} \boldsymbol{\varepsilon}^I &= [\varepsilon_{11}^I \ \varepsilon_{22}^I \ \varepsilon_{33}^I \ 2\varepsilon_{12}^I \ 2\varepsilon_{13}^I \ 2\varepsilon_{23}^I]^T, & \mathbf{E}^I &= [E_1^I \ E_2^I \ E_3^I]^T \\ \boldsymbol{\sigma}^I &= [\sigma_{11}^I \ \sigma_{22}^I \ \sigma_{33}^I \ \sigma_{12}^I \ \sigma_{13}^I \ \sigma_{23}^I]^T, & \mathbf{D}^I &= [D_1^I \ D_2^I \ D_3^I]^T \\ \mathbf{C} &= \begin{bmatrix} C_{1111} & C_{1122} & C_{1133} & C_{1112} & 0 & 0 \\ C_{2211} & C_{2222} & C_{2233} & C_{2212} & 0 & 0 \\ C_{3311} & C_{3322} & C_{3333} & C_{3312} & 0 & 0 \\ C_{1211} & C_{1222} & C_{1233} & C_{1212} & 0 & 0 \\ 0 & 0 & 0 & 0 & C_{1313} & C_{1323} \\ 0 & 0 & 0 & 0 & C_{2313} & C_{2323} \end{bmatrix} \\ \mathbf{e} &= \begin{bmatrix} 0 & 0 & 0 & 0 & e_{113} & e_{123} \\ 0 & 0 & 0 & 0 & e_{213} & e_{223} \\ e_{311} & e_{322} & e_{333} & e_{312} & 0 & 0 \end{bmatrix} \\ \boldsymbol{\varepsilon} &= \begin{bmatrix} \varepsilon_{11} & \varepsilon_{12} & 0 \\ \varepsilon_{21} & \varepsilon_{22} & 0 \\ 0 & 0 & \varepsilon_{33} \end{bmatrix} \end{aligned} \quad (15)$$

where C_{ijkl} , e_{kij} , and ε_{ij} are the elastic, piezoelectric, and dielectric constants.

Substituting through-thickness distributions (4), (5), (7), and (8) in the electroelastic energy (Carrera et al., 2011), one obtains

$$H = \frac{1}{2} \iint_{\Omega} \sum_I \sum_J \Lambda^{IJ} [(\boldsymbol{\sigma}^I)^T \boldsymbol{\varepsilon}^J - (\mathbf{D}^I)^T \mathbf{E}^J] A_1 A_2 d\theta_1 d\theta_2 \quad (16)$$

where Λ^{IJ} are the weighted coefficients defined as

$$\Lambda^{IJ} = \int_{-h/2}^{h/2} L^I L^J c_1 c_2 d\theta_3 \quad (17)$$

The use of equations (13), (14), and (16) leads to a final form of the electroelastic energy in terms of SaS variables

$$\begin{aligned} H &= \iint_{\Omega} \sum_I \sum_J \Lambda^{IJ} \\ &\left[\frac{1}{2} (\boldsymbol{\varepsilon}^I)^T \mathbf{C} \boldsymbol{\varepsilon}^J - (\mathbf{E}^I)^T \mathbf{e} \boldsymbol{\varepsilon}^J - \frac{1}{2} (\mathbf{E}^I)^T \boldsymbol{\varepsilon} \mathbf{E}^J \right] A_1 A_2 d\theta_1 d\theta_2 \end{aligned} \quad (18)$$

4. Hybrid-mixed finite element formulation

To develop the hybrid-mixed piezoelectric solid-shell element formulation, we introduce the displacement-independent strains η_{ij} and assume that they are distributed through the thickness of the shell according to displacement-dependent strain distribution (equation 4)

$$\eta_{ij} = \sum_r L^r \eta_{ij}^r, \quad \eta_{ij}^r = \eta_{ij}(\theta_3^r) \quad (19)$$

where $\eta_{ij}^r(\theta_1, \theta_2)$ are the displacement-independent strains of SaS.

Taking into account equations (18) and (19), the Hu-Washizu variational principle of piezoelectricity (Kulikov and Plotnikova, 2008) can be represented as follows

$$\begin{aligned} & \delta \iint_{\Omega} \sum_I \sum_J \Lambda^{IJ} \left[\frac{1}{2} (\boldsymbol{\eta}^J)^T \mathbf{C} \boldsymbol{\eta}^J - (\mathbf{E}^I)^T \mathbf{e} \boldsymbol{\eta}^J \right. \\ & \left. - \frac{1}{2} (\mathbf{E}^I)^T \in \mathbf{E}^J - (\boldsymbol{\sigma}^J)^T (\boldsymbol{\eta}^J - \boldsymbol{\varepsilon}^J) \right] A_1 A_2 d\theta_1 d\theta_2 = \delta W \end{aligned} \quad (20)$$

where $\boldsymbol{\eta}^I = [\eta_{11}^I \ \eta_{22}^I \ \eta_{33}^I \ 2\eta_{12}^I \ 2\eta_{13}^I \ 2\eta_{23}^I]^T$ are displacement-independent strain vectors of SaS; W is the work done by electromechanical loads applied to the outer surfaces Ω^- and Ω^+

$$\begin{aligned} W &= \iint_{\Omega} \left((\mathbf{p}^+)^T \mathbf{u}^N - Q^+ \phi^N \right) A_1 A_2 c_1^+ c_2^+ d\theta_1 d\theta_2 \\ &- \iint_{\Omega} \left((\mathbf{p}^-)^T \mathbf{u}^1 + Q^- \phi^1 \right) A_1 A_2 c_1^- c_2^- d\theta_1 d\theta_2 + \hat{W} \end{aligned} \quad (21)$$

where $\mathbf{p}^- = [p_1^- \ p_2^- \ p_3^-]^T$ and $\mathbf{p}^+ = [p_1^+ \ p_2^+ \ p_3^+]^T$ are the traction vectors on the outer surfaces; Q^- and Q^+ are the charge densities per unit area of outer surfaces; $\mathbf{u}^1 = [u_1^1 \ u_2^1 \ u_3^1]^T$ and $\mathbf{u}^N = [u_1^N \ u_2^N \ u_3^N]^T$ are the displacement vectors of outer surfaces; ϕ^1 and ϕ^N are the electric potentials of outer surfaces; $c_{\alpha}^- = 1 - k_{\alpha} h/2$ and $c_{\alpha}^+ = 1 + k_{\alpha} h/2$ are the components of the shifter tensor on the outer surfaces; \hat{W} is the work done by external electromechanical loads applied to the boundary surface.

The GeX piezoelectric solid-shell element formulation is based on the use of the bilinear interpolations of displacements and electric potentials of SaS

$$u_i^I = \sum_r N_r u_i^r \quad (22)$$

$$\phi^I = \sum_r N_r \phi_r^I \quad (23)$$

where $N_r(\xi_1, \xi_2)$ are the bilinear shape functions; u_{ir}^I and ϕ_r^I are the displacements and electric potentials of SaS at element nodes; ξ_1, ξ_2 are the normalized curvilinear coordinates θ_1, θ_2 (Figure 2); the nodal index r runs from 1 to 4.

To perform effective analytical integration throughout the solid-shell element, the extended ANS method (Kulikov and Plotnikova, 2015) can be applied

$$\boldsymbol{\varepsilon}^I = \sum_r N_r \boldsymbol{\varepsilon}_r^I, \quad \boldsymbol{\varepsilon}_r^I = [\varepsilon_{11r}^I \ \varepsilon_{22r}^I \ \varepsilon_{33r}^I \ 2\varepsilon_{12r}^I \ 2\varepsilon_{13r}^I \ 2\varepsilon_{23r}^I]^T \quad (24)$$

$$\mathbf{E}^I = \sum_r N_r \mathbf{E}_r^I, \quad \mathbf{E}_r^I = [E_{1r}^I \ E_{2r}^I \ E_{3r}^I]^T \quad (25)$$

where ε_{ijr}^I and E_{ir}^I are the strains and electric field of SaS at element nodes.

This method can be traced back to the ANS method widely used in the literature to circumvent shear, membrane, and curvature thickness locking in isoparametric finite elements (Bathe and Dvorkin, 1986; Betsch and Stein, 1995; Hughes and Tezduyar, 1981; Ko et al., 2017; MacNeal, 1982; Park and Stanley, 1986). However, we treat the term ANS in a broader sense. In the proposed GeX four-node piezoelectric solid-shell element formulation, all components of the displacement-dependent strain tensor and electric field are assumed to vary bilinearly inside the biunit square in (ξ_1, ξ_2) -space. This implies that instead of expected nonlinear interpolations because of equations (10)–(12) the more suitable bilinear interpolations (24) and (25) are employed.

The SaS strains at element nodes are written as

$$\boldsymbol{\varepsilon}_r^I = \mathbf{B}_{ur}^I \mathbf{q} \quad (26)$$

$$\begin{aligned} \mathbf{q} &= [\mathbf{q}_1^T \ \mathbf{q}_2^T \ \mathbf{q}_3^T \ \mathbf{q}_4^T]^T, \\ \mathbf{q}_r &= [u_{1r}^1 \ u_{2r}^1 \ u_{3r}^1 \ u_{1r}^2 \ u_{2r}^2 \ u_{3r}^2 \ \dots \ u_{1r}^N \ u_{2r}^N \ u_{3r}^N]^T \end{aligned} \quad (27)$$

where \mathbf{B}_{ur}^I are the constant matrices of order $6 \times 12N$; \mathbf{q} is the element displacement vector of order $12N$.

The electric field vectors of SaS at element nodes are given by

$$\mathbf{E}_r^I = -\mathbf{B}_{\phi r}^I \boldsymbol{\Phi} \quad (28)$$

$$\boldsymbol{\Phi} = [\boldsymbol{\Phi}_1^T \ \boldsymbol{\Phi}_2^T \ \boldsymbol{\Phi}_3^T \ \boldsymbol{\Phi}_4^T]^T, \quad \boldsymbol{\Phi}_r = [\phi_r^1 \ \phi_r^2 \ \dots \ \phi_r^N]^T \quad (29)$$

where $\mathbf{B}_{\phi r}^I$ are the constant matrices of order $3 \times 4N$; $\boldsymbol{\Phi}$ is the element electric potential vector of order $4N$.

Furthermore, it is convenient to rewrite the ANS interpolation (24) in the following form

$$\boldsymbol{\varepsilon}^I = \sum_{r_1, r_2} (\xi_1)^{r_1} (\xi_2)^{r_2} \boldsymbol{\varepsilon}_{r_1 r_2}^I, \quad \boldsymbol{\varepsilon}_{r_1 r_2}^I = \mathbf{B}_{ur_1 r_2}^I \mathbf{q} \quad (30)$$

where

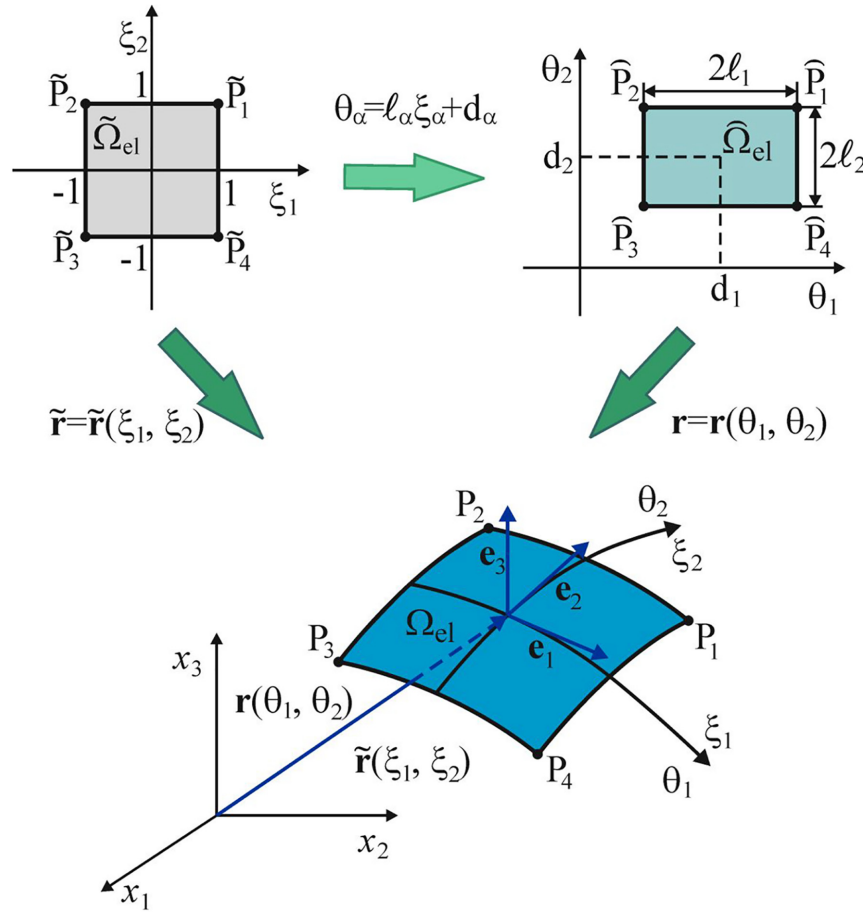


Figure 2. Biunit square in (ξ_1, ξ_2) -space mapped into the middle surface of the GeX four-node solid-shell element in (x_1, x_2, x_3) -space.

$$\boldsymbol{\varepsilon}_{r_1 r_2}^I = \left[\varepsilon_{11r_1 r_2}^I \quad \varepsilon_{22r_1 r_2}^I \quad \varepsilon_{33r_1 r_2}^I \quad 2\varepsilon_{12r_1 r_2}^I \quad 2\varepsilon_{13r_1 r_2}^I \quad 2\varepsilon_{23r_1 r_2}^I \right]^T \quad (31)$$

$$\mathbf{B}_{u00}^I = \frac{1}{4} (\mathbf{B}_{u1}^I + \mathbf{B}_{u2}^I + \mathbf{B}_{u3}^I + \mathbf{B}_{u4}^I)$$

$$\mathbf{B}_{u01}^I = \frac{1}{4} (\mathbf{B}_{u1}^I + \mathbf{B}_{u2}^I - \mathbf{B}_{u3}^I - \mathbf{B}_{u4}^I)$$

$$\mathbf{B}_{u10}^I = \frac{1}{4} (\mathbf{B}_{u1}^I - \mathbf{B}_{u2}^I - \mathbf{B}_{u3}^I + \mathbf{B}_{u4}^I)$$

$$\mathbf{B}_{u11}^I = \frac{1}{4} (\mathbf{B}_{u1}^I - \mathbf{B}_{u2}^I + \mathbf{B}_{u3}^I - \mathbf{B}_{u4}^I)$$

$$\mathbf{B}_{\phi 00}^I = \frac{1}{4} (\mathbf{B}_{\phi 1}^I + \mathbf{B}_{\phi 2}^I + \mathbf{B}_{\phi 3}^I + \mathbf{B}_{\phi 4}^I)$$

$$\mathbf{B}_{\phi 01}^I = \frac{1}{4} (\mathbf{B}_{\phi 1}^I + \mathbf{B}_{\phi 2}^I - \mathbf{B}_{\phi 3}^I - \mathbf{B}_{\phi 4}^I)$$

$$\mathbf{B}_{\phi 10}^I = \frac{1}{4} (\mathbf{B}_{\phi 1}^I - \mathbf{B}_{\phi 2}^I - \mathbf{B}_{\phi 3}^I + \mathbf{B}_{\phi 4}^I)$$

$$\mathbf{B}_{\phi 11}^I = \frac{1}{4} (\mathbf{B}_{\phi 1}^I - \mathbf{B}_{\phi 2}^I + \mathbf{B}_{\phi 3}^I - \mathbf{B}_{\phi 4}^I)$$

Here and below, the indices r_1 and r_2 run from 0 to 1.

To prevent shear and membrane locking and have no spurious zero-energy modes (Kulikov et al., 2018), the displacement-independent strain interpolation is utilized

$$\boldsymbol{\eta}^I = \sum_{r_1 + r_2 < 2} (\xi_1)^{r_1} (\xi_2)^{r_2} \mathbf{Q}_{r_1 r_2} \boldsymbol{\eta}_{r_1 r_2}^I \quad (34)$$

$$\boldsymbol{\eta}_{00}^I = [\psi_1^I \quad \psi_2^I \quad \psi_3^I \quad \psi_4^I \quad \psi_5^I \quad \psi_6^I]^T$$

$$\boldsymbol{\eta}_{01}^I = [\psi_7^I \quad \psi_9^I \quad \psi_{11}^I]^T, \quad \boldsymbol{\eta}_{10}^I = [\psi_8^I \quad \psi_{10}^I \quad \psi_{12}^I]^T$$

where $\mathbf{Q}_{r_1 r_2}$ are the projective matrices given by

The same modification concerns the ANS interpolation (25)

$$\mathbf{E}^I = \sum_{r_1, r_2} (\xi_1)^{r_1} (\xi_2)^{r_2} \mathbf{E}_{r_1 r_2}^I, \quad \mathbf{E}_{r_1 r_2}^I = -\mathbf{B}_{\phi r_1 r_2}^I \boldsymbol{\Phi} \quad (32)$$

where

$$\mathbf{E}_{r_1 r_2}^I = [E_{1r_1 r_2}^I \quad E_{2r_1 r_2}^I \quad E_{3r_1 r_2}^I]^T \quad (33)$$

$$\mathbf{Q}_{00} = \begin{bmatrix} 1 & 0 & 0 & 0 & 0 & 0 \\ 0 & 1 & 0 & 0 & 0 & 0 \\ 0 & 0 & 1 & 0 & 0 & 0 \\ 0 & 0 & 0 & 1 & 0 & 0 \\ 0 & 0 & 0 & 0 & 1 & 0 \\ 0 & 0 & 0 & 0 & 0 & 1 \end{bmatrix} \quad (35)$$

$$\mathbf{Q}_{01} = \begin{bmatrix} 1 & 0 & 0 \\ 0 & 0 & 0 \\ 0 & 1 & 0 \\ 0 & 0 & 0 \\ 0 & 0 & 1 \\ 0 & 0 & 0 \end{bmatrix}, \quad \mathbf{Q}_{10} = \begin{bmatrix} 0 & 0 & 0 \\ 1 & 0 & 0 \\ 0 & 1 & 0 \\ 0 & 0 & 0 \\ 0 & 0 & 0 \\ 0 & 0 & 1 \end{bmatrix}$$

The similar interpolation is accepted for stresses

$$\boldsymbol{\sigma}^I = \sum_{r_1 + r_2 < 2} (\xi_1)^{r_1} (\xi_2)^{r_2} \mathbf{Q}_{r_1 r_2} \boldsymbol{\sigma}_{r_1 r_2}^I \quad (36)$$

$$\boldsymbol{\sigma}_{00}^I = [\mu_1^I \ \mu_2^I \ \mu_3^I \ \mu_4^I \ \mu_5^I \ \mu_6^I]^T$$

$$\boldsymbol{\sigma}_{01}^I = [\mu_7^I \ \mu_9^I \ \mu_{11}^I]^T, \quad \boldsymbol{\sigma}_{10}^I = [\mu_8^I \ \mu_{10}^I \ \mu_{12}^I]^T$$

Substituting interpolations (22), (23), (30), (32), (34), and (36) in the Hu-Washizu variational equations (20) and (21), replacing the metric product $A_1 A_2$ in surface integrals by its value at the element center and integrating analytically throughout the finite element, one can derive the element equilibrium equations. Eliminating then strain and stress parameters ψ_l^I and μ_l^I ($l = 1, 2, \dots, 12$), the following linear equations of the GeX hybrid-mixed four-node solid-shell element are obtained

$$\begin{bmatrix} \mathbf{K}_{uu} & \mathbf{K}_{u\phi} \\ \mathbf{K}_{\phi u} & \mathbf{K}_{\phi\phi} \end{bmatrix} \begin{bmatrix} \mathbf{q} \\ \boldsymbol{\Phi} \end{bmatrix} = \begin{bmatrix} \mathbf{F}_u \\ \mathbf{F}_\phi \end{bmatrix} \quad (37)$$

where \mathbf{K}_{uu} , $\mathbf{K}_{u\phi}$, $\mathbf{K}_{\phi u} = \mathbf{K}_{u\phi}^T$, and $\mathbf{K}_{\phi\phi}$ are the mechanical, piezoelectric, and dielectric stiffness matrices; \mathbf{F}_u and \mathbf{F}_ϕ are the element-wise mechanical and electric surface vectors given by

$$\mathbf{K}_{uu} = \sum_I \sum_J \Lambda^{IJ} \sum_{r_1 + r_2 < 2} \frac{1}{3^{r_1 + r_2}} (\mathbf{B}_{ur_1 r_2}^I)^T \mathbf{Q}_{r_1 r_2} \mathbf{Q}_{r_1 r_2}^T \mathbf{C} \mathbf{Q}_{r_1 r_2} \mathbf{Q}_{r_1 r_2}^T \mathbf{B}_{ur_1 r_2}^J \quad (38)$$

$$\mathbf{K}_{u\phi} = \sum_I \sum_J \Lambda^{IJ} \sum_{r_1 + r_2 < 2} \frac{1}{3^{r_1 + r_2}} (\mathbf{B}_{ur_1 r_2}^I)^T \mathbf{Q}_{r_1 r_2} \mathbf{Q}_{r_1 r_2}^T \mathbf{e}^T \mathbf{B}_{\phi r_1 r_2}^J$$

$$\mathbf{K}_{\phi\phi} = - \sum_I \sum_J \Lambda^{IJ} \sum_{r_1 + r_2 \leq 2} \frac{1}{3^{r_1 + r_2}} (\mathbf{B}_{\phi r_1 r_2}^I)^T \in \mathbf{B}_{\phi r_1 r_2}^J$$

$$\mathbf{F}_u = [\mathbf{F}_{u1}^T \ \mathbf{F}_{u2}^T \ \mathbf{F}_{u3}^T \ \mathbf{F}_{u4}^T]^T, \quad \mathbf{F}_w = [f_{1r}^- \ f_{2r}^- \ f_{3r}^- \ 0 \ 0 \dots \ 0 \ f_{1r}^+ \ f_{2r}^+ \ f_{3r}^+]^T$$

$$\mathbf{F}_\phi = [\mathbf{F}_{\phi 1}^T \ \mathbf{F}_{\phi 2}^T \ \mathbf{F}_{\phi 3}^T \ \mathbf{F}_{\phi 4}^T]^T, \quad \mathbf{F}_{\phi r} = [g_r^- \ 0 \ 0 \dots \ 0 \ g_r^+]^T$$

where

$$f_{ir}^- = - \int_{-1}^1 \int_{-1}^1 N_r p_i^- c_1^- c_2^- d\xi_1 d\xi_2 \quad (39)$$

$$f_{ir}^+ = \int_{-1}^1 \int_{-1}^1 N_r p_i^+ c_1^+ c_2^+ d\xi_1 d\xi_2$$

$$g_r^- = - \int_{-1}^1 \int_{-1}^1 N_r Q^- c_1^- c_2^- d\xi_1 d\xi_2$$

$$g_r^+ = - \int_{-1}^1 \int_{-1}^1 N_r Q^+ c_1^+ c_2^+ d\xi_1 d\xi_2$$

It is worth noting that all stiffness matrices are evaluated without the expensive numerical matrix inversion that is impossible in available isoparametric hybrid-mixed finite element formulations (Hoa and Feng, 1998).

The equilibrium equations (37) for each element are assembled by a standard technique to form the global equilibrium equations. To manage the mechanical and electric boundary conditions, the common algorithms (Zienkiewicz and Taylor, 2000) can be applied.

5. Numerical examples

The developed GeX four-node piezoelectric solid-shell element is evaluated through two benchmarks to demonstrate its ability to analyze piezoelectric devices accurately. Then it is applied to the analysis and modeling of piezoelectric spiral actuators.

5.1. Eigenvalue problem

In the first example, the eigenvalues of a piezoelectric sample are investigated. This example is employed to verify that the proposed hybrid-mixed solid-shell element does not suffer from the zero-energy modes. The similar testing of the isoparametric six-parameter hybrid-mixed element has been carried out by Klinkel and Wagner (2008). Here, a piezoelectric rectangular parallelepiped with the edge lengths of 2 cm \times 2 cm \times 0.2 cm is considered. The material properties are taken as follows (Klinkel and Wagner, 2008)

$$E_1 = E_2 = 0.0062 \text{ GN/cm}^2, \quad E_3 = 0.0054 \text{ GN/cm}^2,$$

$$\nu_{12} = \nu_{13} = \nu_{23} = 0.31$$

$$G_{12} = 0.0018 \text{ GN/cm}^2, \quad G_{13} = G_{23} = 0.00236 \text{ GN/cm}^2,$$

$$\epsilon_{11} = \epsilon_{22} = \epsilon_{33} = 0.0023 \text{ C}^2/\text{GN} \cdot \text{cm}^2$$

$$e_{311} = e_{322} = -0.0012 \text{ C/cm}^2, \quad e_{333} = 0.00173 \text{ C/cm}^2,$$

$$e_{113} = e_{223} = 0.00158 \text{ C/cm}^2$$

Table 1. Eigenvalues of a piezoelectric rectangular parallelepiped with three SaS.

No.	Eigenvalue	No.	Eigenvalue	No.	Eigenvalue	No.	Eigenvalue
1	$1.9 \cdot 10^{-19}$	13	$-8.8 \cdot 10^{-3}$	25	$9.2 \cdot 10^{-5}$	37	$2.4 \cdot 10^{-2}$
2	$4.6 \cdot 10^{-18}$	14	$-1.0 \cdot 10^{-2}$	26	$9.2 \cdot 10^{-5}$	38	$2.4 \cdot 10^{-2}$
3	$8.3 \cdot 10^{-18}$	15	$-2.6 \cdot 10^{-2}$	27	$1.6 \cdot 10^{-4}$	39	$2.5 \cdot 10^{-2}$
4	$9.0 \cdot 10^{-18}$	16	$-3.5 \cdot 10^{-2}$	28	$1.9 \cdot 10^{-4}$	40	$2.5 \cdot 10^{-2}$
5	$2.1 \cdot 10^{-17}$	17	$-3.5 \cdot 10^{-2}$	29	$2.4 \cdot 10^{-4}$	41	$3.1 \cdot 10^{-2}$
6	$3.0 \cdot 10^{-17}$	18	$-1.0 \cdot 10^{-1}$	30	$3.0 \cdot 10^{-4}$	42	$3.2 \cdot 10^{-2}$
7	$3.8 \cdot 10^{-17}$	19	$1.6 \cdot 10^{-7}$	31	$3.0 \cdot 10^{-4}$	43	$7.5 \cdot 10^{-2}$
8	$-1.5 \cdot 10^{-4}$	20	$1.5 \cdot 10^{-6}$	32	$3.9 \cdot 10^{-4}$	44	$9.5 \cdot 10^{-2}$
9	$-2.2 \cdot 10^{-4}$	21	$4.3 \cdot 10^{-5}$	33	$5.2 \cdot 10^{-4}$	45	$9.5 \cdot 10^{-2}$
10	$-2.2 \cdot 10^{-4}$	22	$4.4 \cdot 10^{-5}$	34	$1.3 \cdot 10^{-3}$	46	$9.9 \cdot 10^{-2}$
11	$-2.6 \cdot 10^{-3}$	23	$4.4 \cdot 10^{-5}$	35	$7.9 \cdot 10^{-3}$	47	$9.9 \cdot 10^{-2}$
12	$-8.8 \cdot 10^{-3}$	24	$7.6 \cdot 10^{-5}$	36	$8.2 \cdot 10^{-3}$	48	$3.0 \cdot 10^{-1}$

Table 2. Eigenvalues of a piezoelectric rectangular parallelepiped with four SaS.

No.	Eigenvalue	No.	Eigenvalue	No.	Eigenvalue	No.	Eigenvalue
1	$3.2 \cdot 10^{-18}$	17	$-8.7 \cdot 10^{-2}$	33	$1.2 \cdot 10^{-4}$	49	$1.6 \cdot 10^{-2}$
2	$6.4 \cdot 10^{-18}$	18	$-8.7 \cdot 10^{-2}$	34	$1.7 \cdot 10^{-4}$	50	$4.8 \cdot 10^{-2}$
3	$1.5 \cdot 10^{-17}$	19	$-9.3 \cdot 10^{-2}$	35	$1.7 \cdot 10^{-4}$	51	$7.8 \cdot 10^{-2}$
4	$2.3 \cdot 10^{-17}$	20	$-9.3 \cdot 10^{-2}$	36	$1.7 \cdot 10^{-4}$	52	$7.9 \cdot 10^{-2}$
5	$2.9 \cdot 10^{-17}$	21	$-2.6 \cdot 10^{-1}$	37	$1.8 \cdot 10^{-4}$	53	$8.4 \cdot 10^{-2}$
6	$5.9 \cdot 10^{-17}$	22	$-2.8 \cdot 10^{-1}$	38	$2.9 \cdot 10^{-4}$	54	$8.5 \cdot 10^{-2}$
7	$1.1 \cdot 10^{-16}$	23	$2.5 \cdot 10^{-8}$	39	$6.6 \cdot 10^{-4}$	55	$2.3 \cdot 10^{-1}$
8	$-1.1 \cdot 10^{-4}$	24	$1.1 \cdot 10^{-7}$	40	$6.6 \cdot 10^{-4}$	56	$2.3 \cdot 10^{-1}$
9	$-1.7 \cdot 10^{-4}$	25	$6.6 \cdot 10^{-6}$	41	$7.3 \cdot 10^{-4}$	57	$2.4 \cdot 10^{-1}$
10	$-1.7 \cdot 10^{-4}$	26	$2.7 \cdot 10^{-5}$	42	$1.2 \cdot 10^{-3}$	58	$2.4 \cdot 10^{-1}$
11	$-1.7 \cdot 10^{-3}$	27	$2.7 \cdot 10^{-5}$	43	$2.8 \cdot 10^{-3}$	59	$2.5 \cdot 10^{-1}$
12	$-5.7 \cdot 10^{-3}$	28	$4.0 \cdot 10^{-5}$	44	$5.1 \cdot 10^{-3}$	60	$2.5 \cdot 10^{-1}$
13	$-5.7 \cdot 10^{-3}$	29	$4.0 \cdot 10^{-5}$	45	$5.5 \cdot 10^{-3}$	61	$2.7 \cdot 10^{-1}$
14	$-1.7 \cdot 10^{-2}$	30	$4.3 \cdot 10^{-5}$	46	$1.5 \cdot 10^{-2}$	62	$2.7 \cdot 10^{-1}$
15	$-2.6 \cdot 10^{-2}$	31	$4.7 \cdot 10^{-5}$	47	$1.5 \cdot 10^{-2}$	63	$7.4 \cdot 10^{-1}$
16	$-2.8 \cdot 10^{-2}$	32	$6.9 \cdot 10^{-5}$	48	$1.6 \cdot 10^{-2}$	64	$7.9 \cdot 10^{-1}$

Tables 1 and 2 list the results of solving the eigenvalue problem taking three and four SaS inside the parallelepiped. As can be seen, there exist seven zero-energy modes exactly for both cases considered, namely six modes related to the rigid body motions and one to the short circuit. All other deformation modes are associated with nonzero eigenvalues. The use of five and more SaS leads to a similar conclusion. Let us pay attention to appearing correspondingly 11 and 15 negative eigenvalues in Tables 1 and 2. This is because of the negative dielectric stiffness matrix of order $4N \times 4N$ given in equation (38). Thus, the developed GeX solid-shell element is free of spurious zero-energy modes at least for the bodies of simple geometry.

5.2. Simply supported piezoelectric cylindrical shell

Consider a simply supported piezoelectric cylindrical shell of the length L subjected to electric loading on the top surface whereas the bottom surface is electrically grounded

$$\phi^- = 0, \quad \phi^+ = \phi_0 \sin \frac{\pi \theta_1}{L} \cos 2\theta_2 \quad (40)$$

where $\phi_0 = 1$ V. The bottom and top surfaces of the shell are assumed to be traction free. The shell is composed of the PZT-4 with the material properties (Heyliger, 1997; Kulikov and Plotnikova, 2013)

$$C_{1111} = C_{2222} = 139.0 \text{ GPa}, \quad C_{3333} = 115.0 \text{ GPa}, \\ C_{1122} = 77.8 \text{ GPa}$$

$$C_{1133} = C_{2233} = 74.3 \text{ GPa}, \quad C_{1313} = C_{2323} = 25.6 \text{ GPa}, \\ C_{1212} = 30.6 \text{ GPa}$$

$$e_{311} = e_{322} = -5.2 \text{ C/m}^2, \quad e_{333} = 15.08 \text{ C/m}^2, \\ e_{113} = e_{223} = 12.72 \text{ C/m}^2$$

$$\epsilon_{11} = \epsilon_{22} = 13.06 \text{ nF/m}, \quad \epsilon_{33} = 11.51 \text{ nF/m}$$

Due to symmetry of the problem (see Figure 3), only one octant of the shell ($0 \leq \theta_1 \leq L/2$, $0 \leq \theta_2 \leq \pi/2$) is modeled by a uniform mesh 48×96 . To analyze the

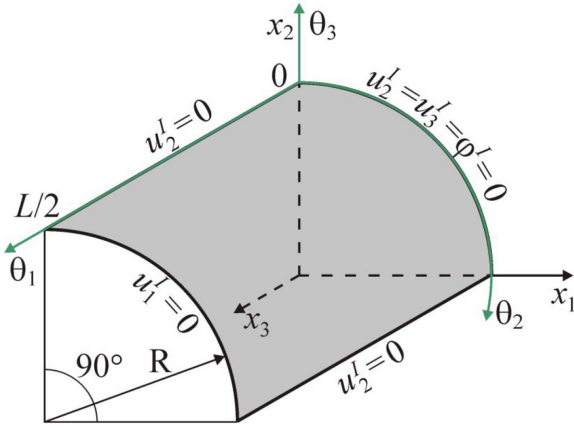


Figure 3. One octant of the piezoelectric cylindrical shell.

results efficiently, we introduce the following scaled variables at crucial points

$$\begin{aligned} \bar{u}_1(z) &= 10^{11} \times u_1(L, 0, z)/S, & \bar{u}_2(z) &= 10^{11} \\ &\times u_2(L/2, \pi/4, z)/S, & \bar{u}_3(z) &= 10^{11} \\ &\times u_3(L/2, 0, z)/S \end{aligned}$$

$$\begin{aligned} \bar{\sigma}_{11}(z) &= 10^{-3} \times \sigma_{11}(L/2, 0, z), & \bar{\sigma}_{22}(z) &= 10^{-3} \\ &\times \sigma_{22}(L/2, 0, z), & \bar{\sigma}_{33}(z) &= 10^{-2} \times S\sigma_{33}(L/2, 0, z) \end{aligned}$$

$$\begin{aligned} \bar{\sigma}_{13}(z) &= 10^{-3} \times S\sigma_{13}(L, 0, z), & \bar{\sigma}_{23}(z) &= 10^{-3} \\ &\times S\sigma_{23}(L/2, \pi/4, z) \end{aligned}$$

$$\begin{aligned} \bar{\varphi}(z) &= \phi(L/2, 0, z), & \bar{D}_3(z) &= 10^6 \times D_3(L/2, 0, z)/S, \\ & & z &= \theta_3/h \end{aligned}$$

where $S = R^+/h$ is the slenderness ratio; R^+ is the radius of the top cylindrical surface.

Tables 3 and 4 list the results of the convergence study for thick and moderately thick cylindrical shells with $L = R^+ = 0.01$ m by increasing a number of SaS N . The obtained results are compared with the exact SaS solution (Kulikov and Plotnikova, 2013). Figure 4 shows the effect of a number of SaS on the through-thickness distributions of transverse components of the stress tensor and electric displacement vector for a thick piezoelectric cylindrical shell with $S = 4$ using a fine 48×96 mesh compared with the exact SaS solution (Kulikov and Plotnikova, 2013). It is seen that the choice of three SaS inside the shell body yields unacceptable results. To satisfy the boundary conditions for the transverse normal stress on outer surfaces, more than five SaS have to be taken. Figures 5 and 6 display the through-thickness distributions of displacements, electric potential, electric displacement, and stresses for different slenderness ratios using five SaS for $S = 10$ and 100, seven SaS for $S = 4$, and nine SaS for $S = 2$ and the same fine mesh. These results demonstrate the high potential of the proposed GeX hybrid-mixed piezoelectric solid-shell element formulation. This is due the fact that the boundary conditions on the bottom and top surfaces for transverse stresses are satisfied with a high accuracy.

The results of the convergence study due to mesh refinement are presented in Figure 7. The analytical answer is provided by the exact SaS solution (Kulikov and Plotnikova, 2013) given in Table 5. Here, we consider regular $4k \times 8k$ meshes, which are characterized by the mesh parameter $k = 1, 2, 4, 8$, and 12. As can be seen, the proposed GeX solid-shell element behaves well in the case of coarse meshes, especially in thin shell limits.

Table 3. Results for a piezoelectric cylindrical shell with $S = 2$ using uniform mesh 48×96 .

N	$\bar{u}_1(0.5)$	$\bar{u}_2(0.5)$	$\bar{u}_3(0)$	$\bar{\varphi}(0)$	$\bar{\sigma}_{22}(0.5)$	$\bar{\sigma}_{13}(0)$	$\bar{\sigma}_{23}(0)$	$\bar{\sigma}_{33}(0)$	$\bar{D}_3(0)$
3	8.722	8.492	-1.644	0.3558	-1.318	-0.672	-0.5463	8.2003	-1.549
5	8.955	8.636	-1.805	0.3648	-2.172	-1.104	-0.8863	0.8709	-1.327
7	8.962	8.638	-1.800	0.3660	-2.278	-1.087	-0.8903	0.7039	-1.339
9	8.962	8.638	-1.801	0.3661	-2.271	-1.087	-0.8920	0.6801	-1.339
11	8.962	8.638	-1.801	0.3660	-2.270	-1.087	-0.8918	0.6816	-1.339
Exact	8.963	8.637	-1.800	0.3660	-2.267	-1.088	-0.8924	0.6816	-1.340

Table 4. Results for a piezoelectric cylindrical shell with $S = 10$ using uniform mesh 48×96 .

N	$\bar{u}_1(0.5)$	$\bar{u}_2(0.5)$	$\bar{u}_3(0)$	$\bar{\varphi}(0)$	$\bar{\sigma}_{22}(0.5)$	$\bar{\sigma}_{13}(0)$	$\bar{\sigma}_{23}(0)$	$\bar{\sigma}_{33}(0)$	$\bar{D}_3(0)$
3	6.091	0.2574	12.14	0.5259	2.499	-5.770	-3.465	-14.00	-1.680
5	6.094	0.2533	12.12	0.5260	2.245	-7.720	-4.498	-11.83	-1.669
7	6.094	0.2533	12.13	0.5260	2.245	-7.716	-4.496	-11.74	-1.669
9	6.094	0.2533	12.13	0.5260	2.245	-7.716	-4.496	-11.74	-1.669
Exact	6.095	0.2527	12.13	0.5260	2.245	-7.719	-4.497	-11.89	-1.670

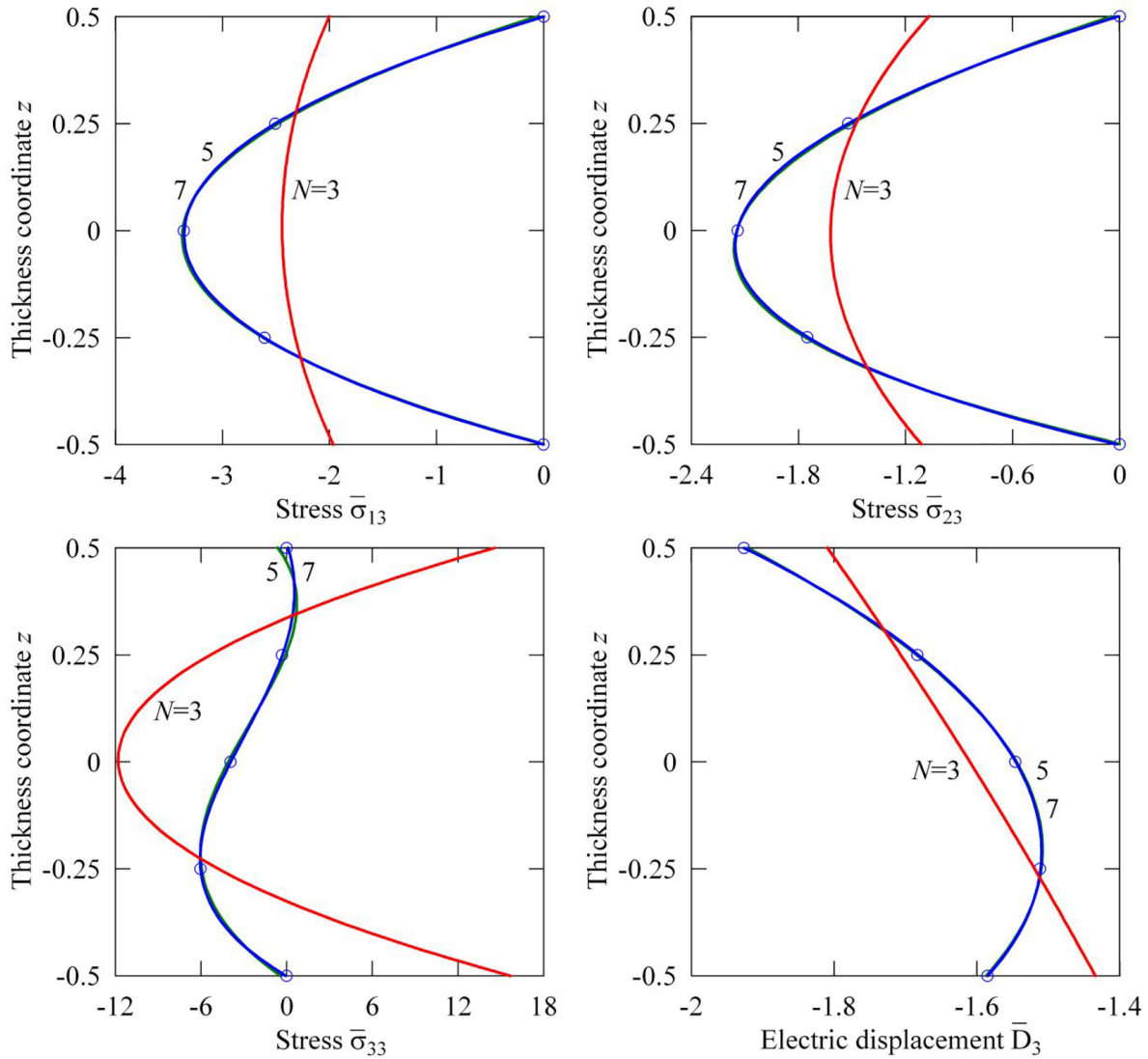


Figure 4. Through-thickness distributions of stresses and electric displacement for a thick piezoelectric cylindrical shell with $S = 4$ using 48×96 mesh compared with the exact SaS solution (Kulikov and Plotnikova, 2013) using seven SaS (\circ).

5.3. Piezoelectric spiral actuator

Consider a spiral actuator consisting of four turns as depicted in Figure 8. The coefficients of the first fundamental form and principal curvatures of the middle surface from strain-displacement equations (10) and (11) are written as follows

$$A_1 = \sqrt{a^2 + r^2}, \quad A_2 = 1, \quad k_1 = \frac{1}{A_1^3} (2a^2 + r^2), \quad k_2 = 0$$

$$r = r_0 + a\theta_1, \quad \theta_1 \in [0, 8\pi]$$
(41)

where r is the polar radius; a is the parameter that controls the distance between successive turnings; r_0 is the initial radius.

The actuator is polarized in the thickness direction and clamped at point $\theta_1 = 0$. In the case of applying the radial electric field in the poling direction, the spiral tip moves in tangential and radial directions. As it turned out, the tangential displacement is much larger than the transverse tip displacement of a piezoelectric strip of the same length under the same voltage (Mohammadi et al., 1999). The tangential tip displacement of the spiral actuator with the effective length $L = 260$ mm, external diameter $d = 30$ mm, thickness $h = 0.95$ mm, and width $b = 3.7$ mm under the applied voltage is shown in Figure 9. The transverse tip displacement of the piezoelectric strip with the same length, thickness, and width is also presented. Both actuators are made of the PZT-5H ceramic. However, its material properties are not documented by Mohammadi et al. (1999). Here,

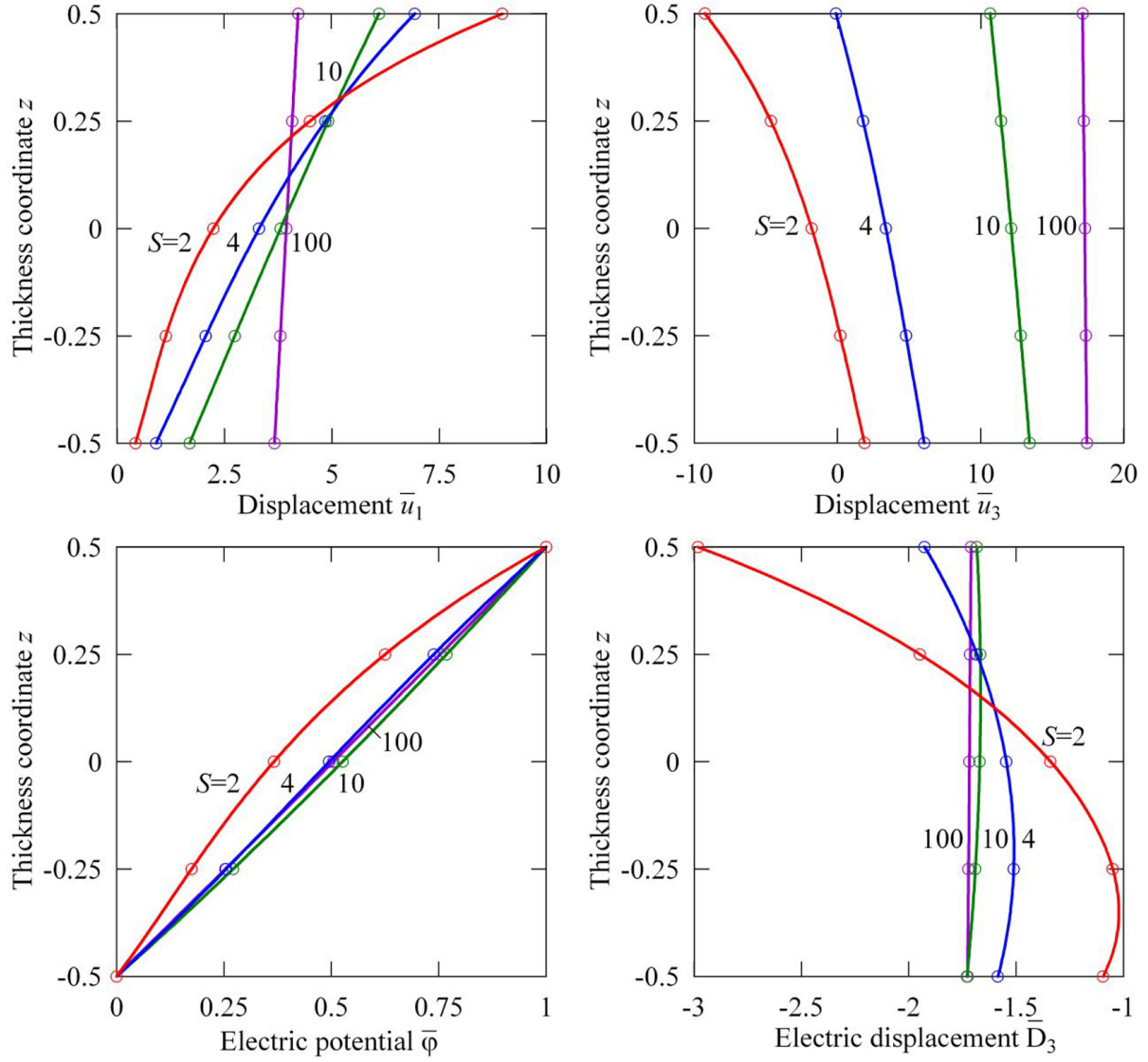


Figure 5. Through-thickness distributions of displacements, electric potential and electric displacement for a piezoelectric cylindrical shell using five SaS for $S = 10$ and 100 , seven SaS for $S = 4$, and nine SaS for $S = 2$ and 48×96 mesh compared with the exact SaS solution (Kulikov and Plotnikova, 2013) using the same number of SaS (\circ).

we consider a PZT-5H with the following material properties (Cheng et al., 2000; Heinonen et al., 2005)

$$E_1 = E_2 = 61 \text{ GPa}, \quad E_3 = 48 \text{ GPa}, \quad \nu_{12} = \nu_{13} = \nu_{23} = 0.31$$

$$G_{12} = 23.3 \text{ GPa}, \quad G_{13} = G_{23} = 19.1 \text{ GPa}, \\ \epsilon_{11} = \epsilon_{22} = 15.052 \text{ nF/m}, \quad \epsilon_{33} = 13.015 \text{ nF/m}$$

$$e_{311} = e_{322} = -14.645 \text{ C/m}^2, \quad e_{333} = 21.319 \text{ C/m}^2, \\ e_{113} = e_{223} = 15.414 \text{ C/m}^2$$

Due to symmetry, only one half of the spiral shell ($0 \leq \theta_1 \leq 8\pi$, $0 \leq \theta_2 \leq b/2$) is modeled by a regular 64×4 mesh of GeX solid-shell elements using five SaS.

The geometrical parameters of the spiral are chosen to be $a = 0.448 \text{ mm/rad}$ and $r_0 = 4.7 \text{ mm}$ that corresponds to spiral geometry of Mohammadi et al. (1999). As expected, the experimental response is nonlinear but for the considered voltage range it is close to linear and, therefore, a good agreement between experimental and numerical results is observed.

For the further analysis, it is convenient to introduce the scaled variables at any point $P(\theta_1, 0)$ belonging to the middle surface as functions of the dimensionless thickness coordinate as follows

$$\bar{u}_1(P, z) = 10^6 \times u_1(P, z), \quad \bar{u}_3(P, z) = 10^6 \times u_3(P, z), \\ \bar{\sigma}_{11}(P, z) = 10^{-3} \times \sigma_{11}(P, z)$$

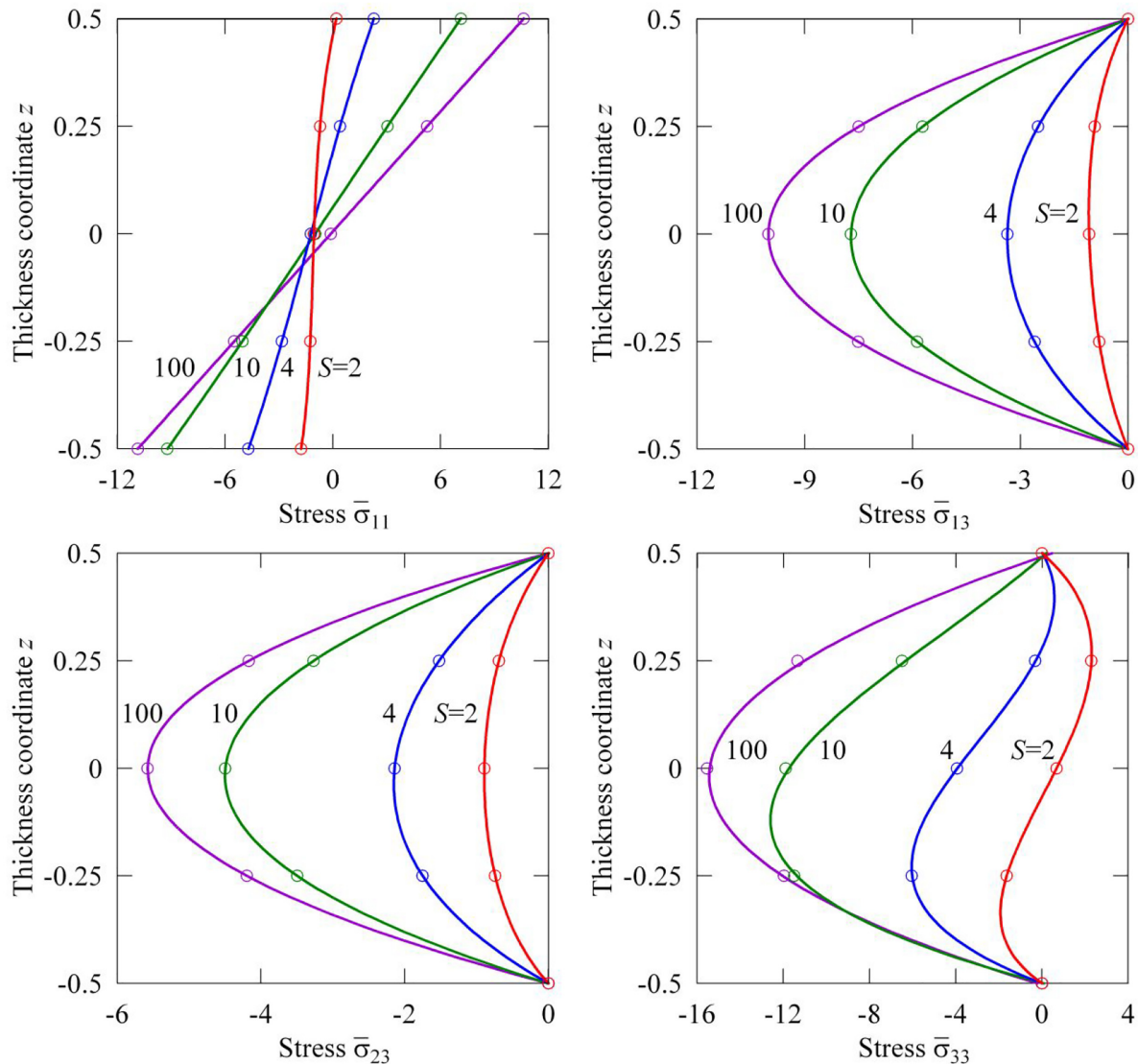


Figure 6. Through-thickness distributions of stresses for a piezoelectric cylindrical shell using five SaS for $S = 10$ and 100 , seven SaS for $S = 4$, and nine SaS for $S = 2$ and 48×96 mesh compared with the exact SaS solution (Kulikov and Plotnikova, 2013) using the same number of SaS (\circ).

$$\begin{aligned} \bar{\sigma}_{22}(\mathbf{P}, z) &= 10^{-3} \times \sigma_{22}(\mathbf{P}, z), \quad \bar{\sigma}_{13}(\mathbf{P}, z) = 10^{-3} \\ &\times \sigma_{13}(\mathbf{P}, z), \quad \bar{\sigma}_{33}(\mathbf{P}, z) = 10^{-3} \times \sigma_{33}(\mathbf{P}, z) \\ \bar{\varphi}(\mathbf{P}, z) &= \phi(\mathbf{P}, z), \quad \bar{D}_3(\mathbf{P}, z) = 10^3 \times D_3(\mathbf{P}, z), \quad z = \theta_3/h \end{aligned}$$

Figures 10 and 11 show the through-thickness distributions of displacements, electric potential, electric displacement, and stresses at points A, B, C, and D using five SaS under the applied voltage of 200 V. These results demonstrate again the high potential of the GeX piezoelectric solid-shell element formulation because boundary conditions on the bottom and top surfaces for transverse stresses are satisfied correctly.

Figure 12 displays the results of the convergence study due to the mesh refinement using regular $K_1 \times K_2$

meshes, where $K_1 = 16k$ is the number of elements in the θ_1 -direction that characterized by the mesh parameter $k = 1, 2, 4, 8$, and K_2 is the number of elements in the θ_2 -direction, that is, across the width. As can be seen, the developed GeX solid-shell element with five SaS behaves excellently for coarse mesh configurations. In particular, the displacements and electric potential can be calculated with a good accuracy by using one or two elements across the width. However, to evaluate stresses well, we have to take not less than eight elements.

Finally, we investigate the effect of a number of spiral turns and the initial radius r_0 on the tangential tip displacement using five SaS and a regular mesh 60×4 . Consider spiral actuators consisting of three,

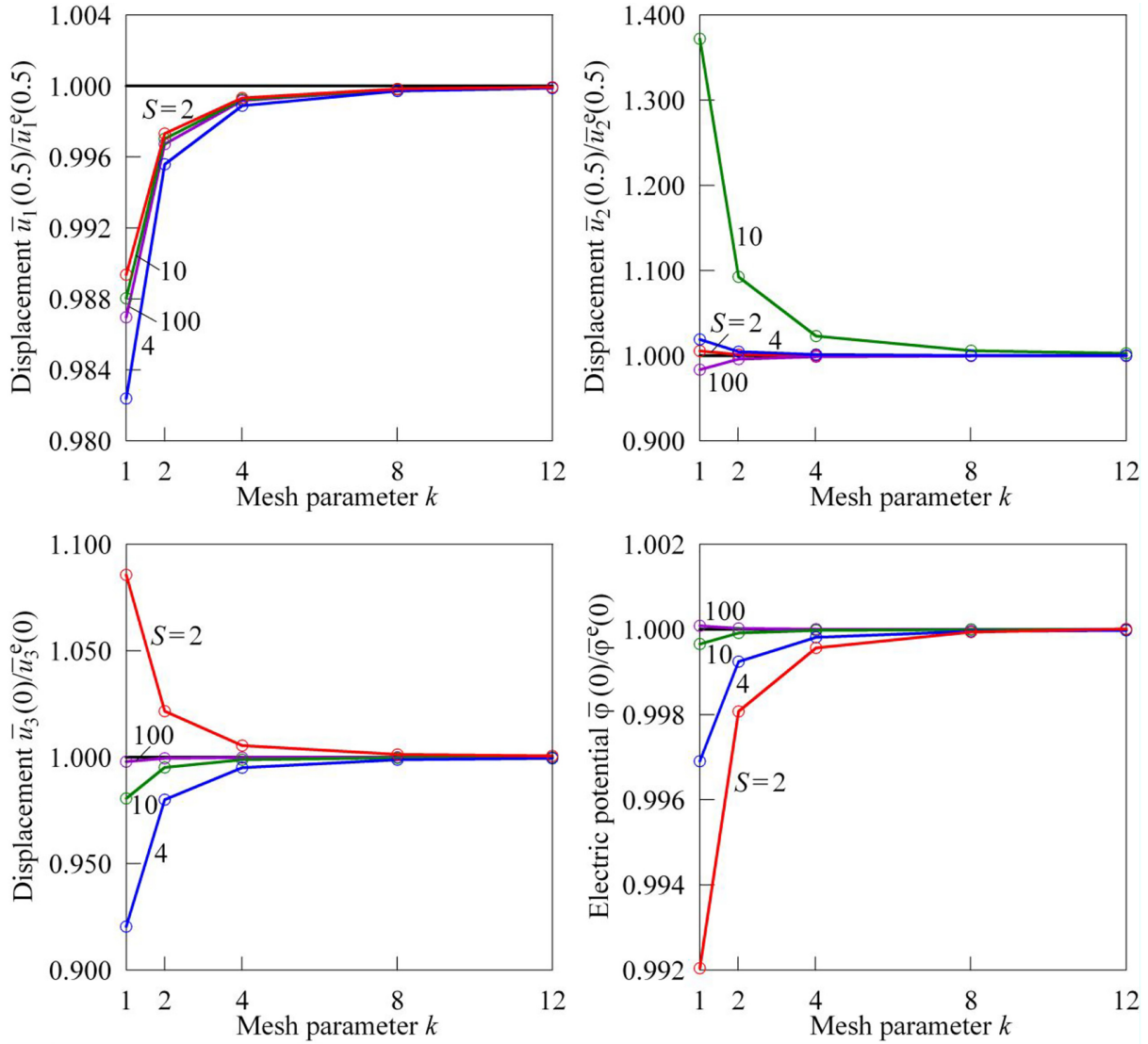


Figure 7. Convergence study due to mesh refinement for a piezoelectric cylindrical shell using five SaS for $S = 10$ and 100 , seven SaS for $S = 4$, and nine SaS for $S = 2$: the reference values are provided by Table 5.

Table 5. Reference values of displacements and electric potential for a piezoelectric cylindrical shell (Kulikov and Plotnikova, 2013) using five SaS for $S = 10$ and 100 , seven SaS for $S = 4$, and nine SaS for $S = 2$.

S	$\bar{u}_1^e(0.5)$	$\bar{u}_2^e(0.5)$	$\bar{u}_3^e(0)$	$\bar{\varphi}^e(0)$
2	8.963	8.637	-1.800	0.3660
4	6.925	3.992	3.386	0.4950
10	6.095	0.2527	12.13	0.5260
100	4.213	-2.338	17.28	0.5042

four, and five turns with $L = 260$ mm, $h = 0.95$ mm, and $b = 3.7$ mm under the applied voltage of 200 V. The initial radius takes eight values from 1.5 to 5 mm in increments of 0.5 mm. The geometric parameters of

the spirals are given in Table 6. The spiral parameter a is found by solving the equation

$$\int_0^{2\pi m} \sqrt{a^2 + r^2} d\theta_1 = L \quad (42)$$

where m is the number of turns. Then, the external diameter d can be defined by

$$d = 2r_0 + h + 2(2m - 1)\pi a \quad (43)$$

Figure 13 shows the tangential tip displacement as a function of the number of turns and the initial radius. It can be seen that spiral actuators with the smallest initial radius have the greatest displacement of the tip.

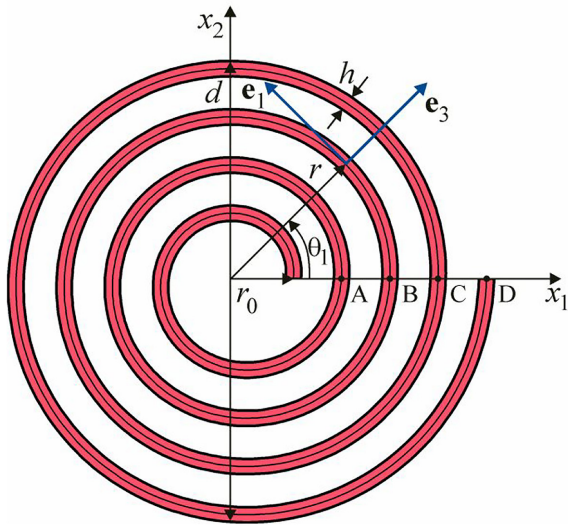


Figure 8. Spiral actuator with four turns.

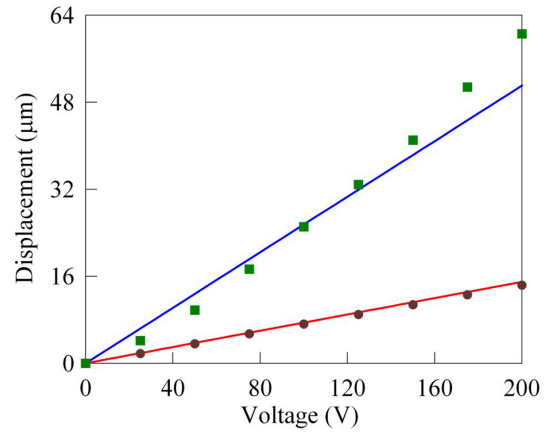


Figure 9. Tangential and transverse tip displacements of spiral and straight actuators, correspondingly, versus an applied voltage: the proposed GeX four-node solid-shell element (solid lines), experimental results (Mohammadi et al., 1999) for a spiral actuator (\square), and numerical results (Mohammadi et al., 1999) for a straight actuator of the same length (\circ).

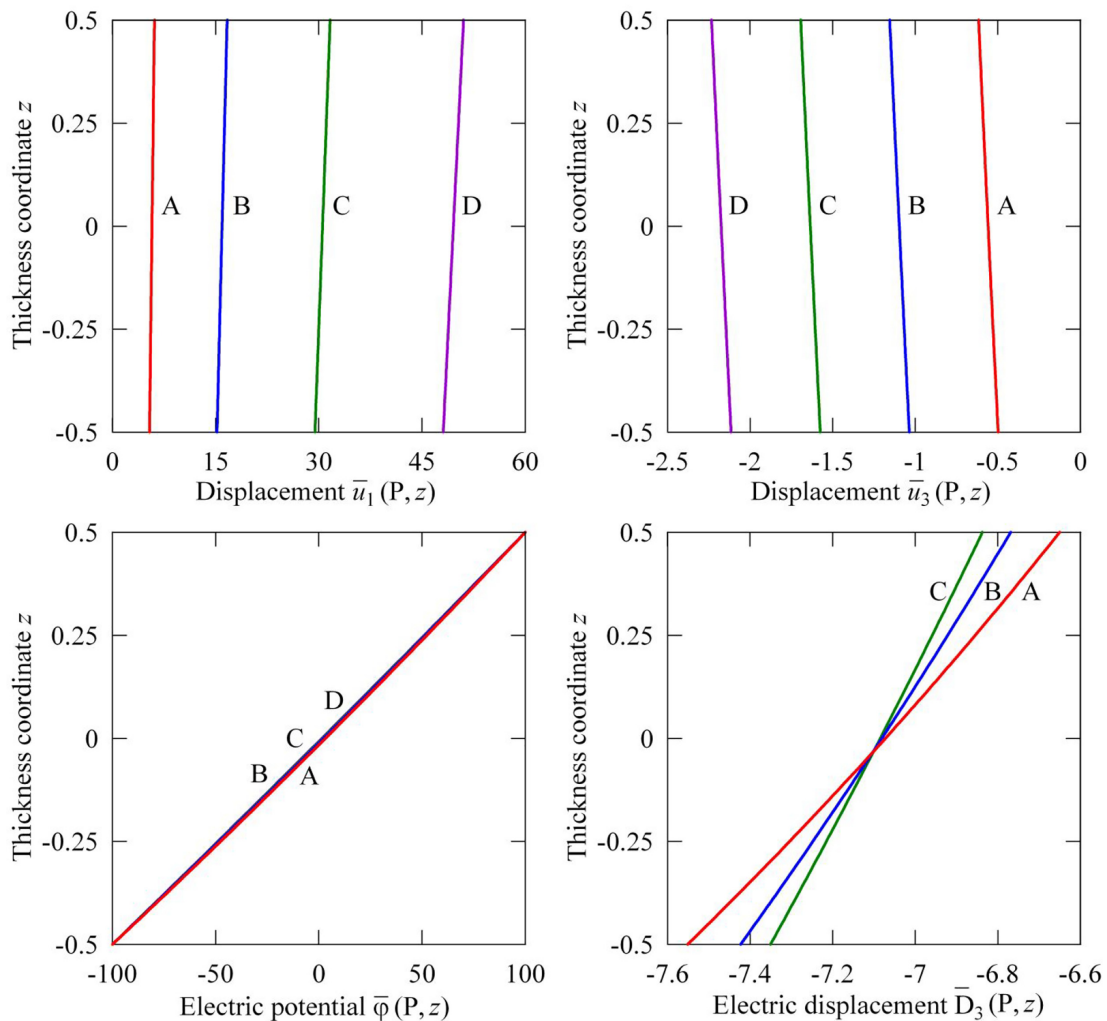


Figure 10. Through-thickness distributions of displacements, electric potential and electric displacement for a spiral actuator at points A, B, C, and D using five SaS and 512×32 mesh.

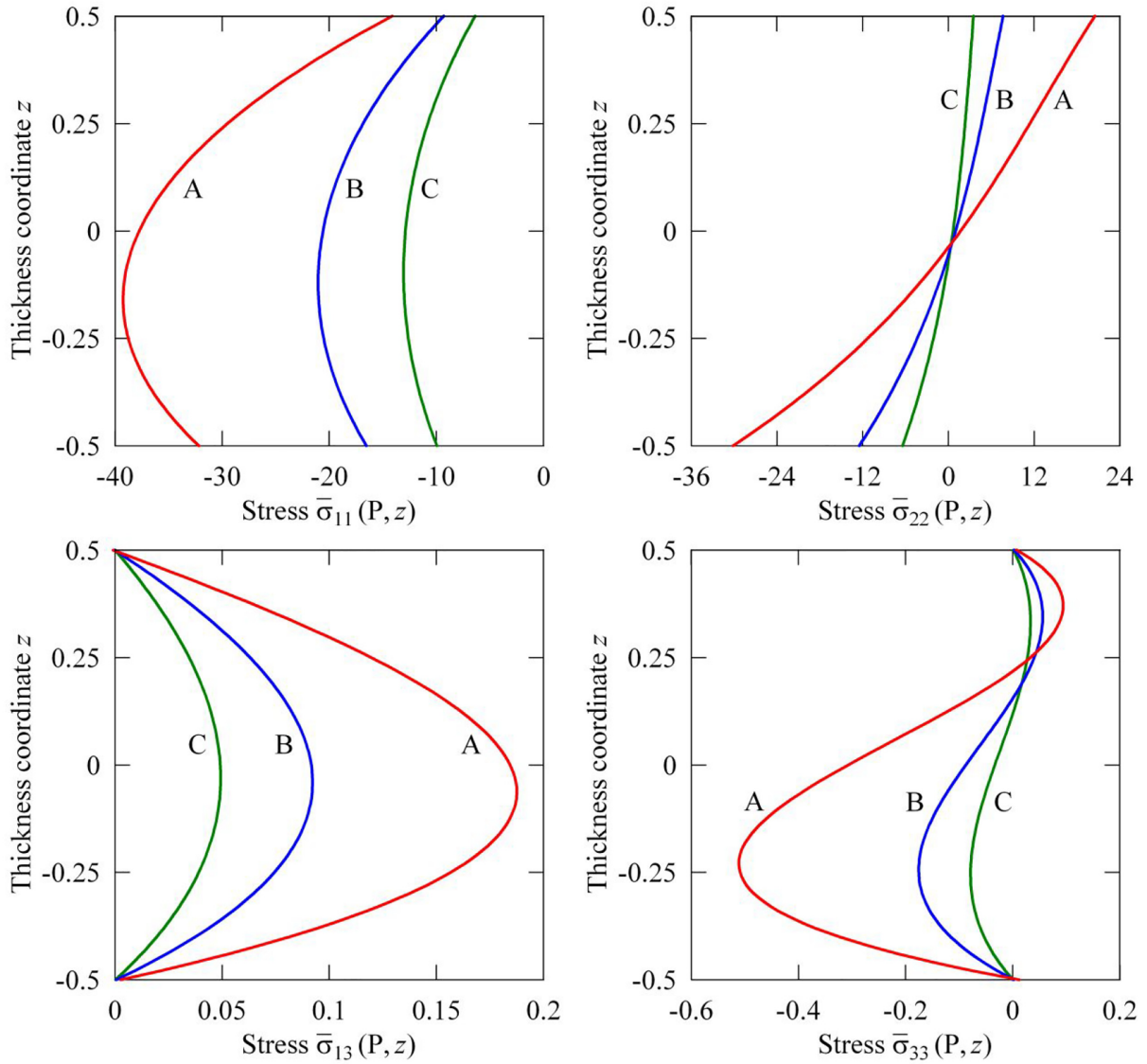


Figure 11. Through-thickness distributions of stresses for a spiral actuator at points A, B, and C using five SaS and 512×32 mesh.

Table 6. Geometry of spirals with a different number of turns.

Spiral with three turns			Spiral with four turns			Spiral with five turns		
r_0 (mm)	a (mm)	d (mm)	r_0 (mm)	a (mm)	d (mm)	r_0 (mm)	a (mm)	d (mm)
1.5	1.294	44.6	1.5	0.7011	34.8	1.5	0.4304	28.3
2.0	1.243	44.0	2.0	0.6618	34.1	2.0	0.3987	27.5
2.5	1.191	43.4	2.5	0.6223	33.3	2.5	0.3671	26.7
3.0	1.139	42.7	3.0	0.5829	32.6	3.0	0.3354	25.9
3.5	1.086	42.1	3.5	0.5433	31.8	3.5	0.3036	25.1
4.0	1.034	41.4	4.0	0.5038	31.1	4.0	0.2719	24.3
4.5	0.9816	40.8	4.5	0.4642	30.4	4.5	0.2402	23.5
5.0	0.9291	40.1	5.0	0.4246	29.6	5.0	0.2084	22.7

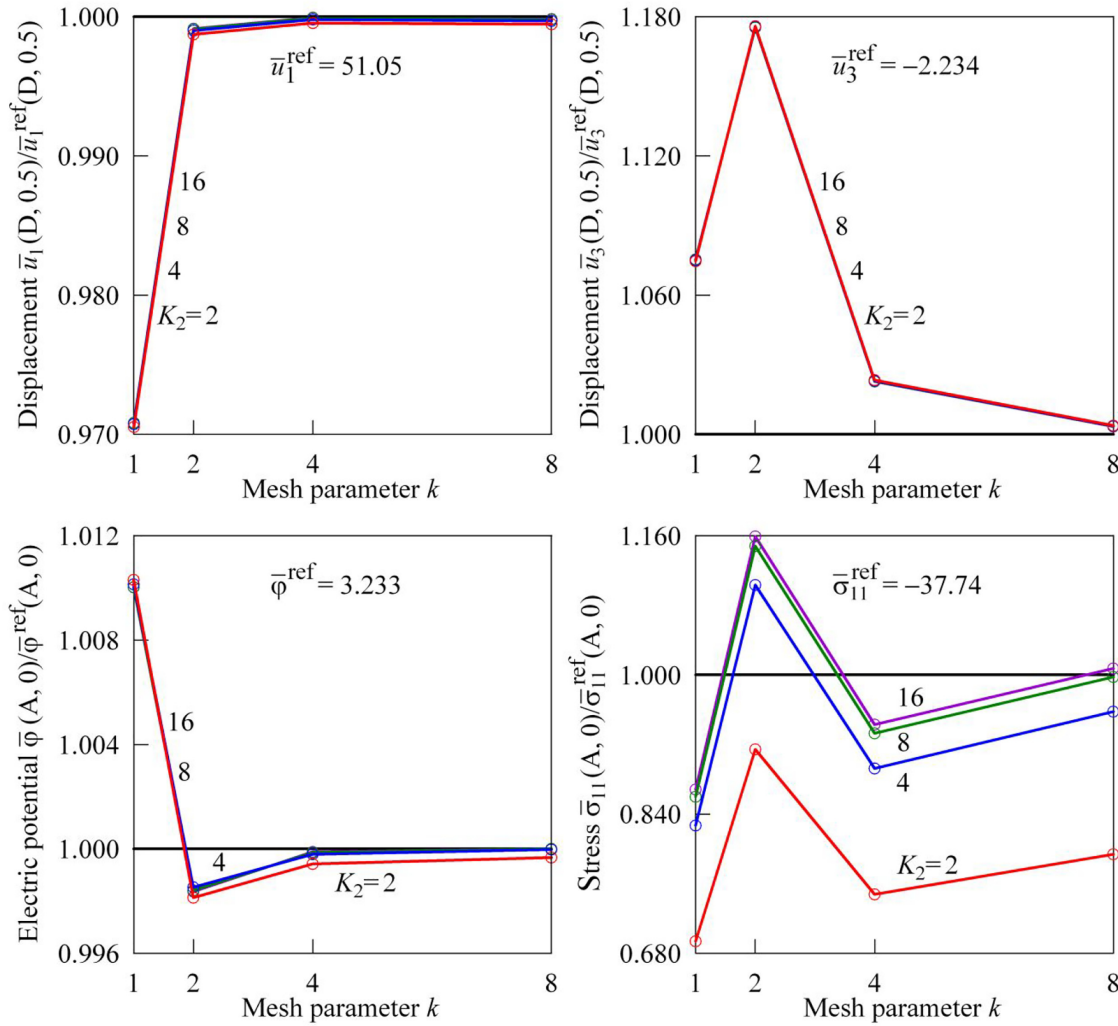


Figure 12. Convergence study due to mesh refinement for a spiral actuator under an applied voltage of 200 V with five SaS using $4k \times K_2$ meshes: the reference values are provided by a fine 512×32 mesh.

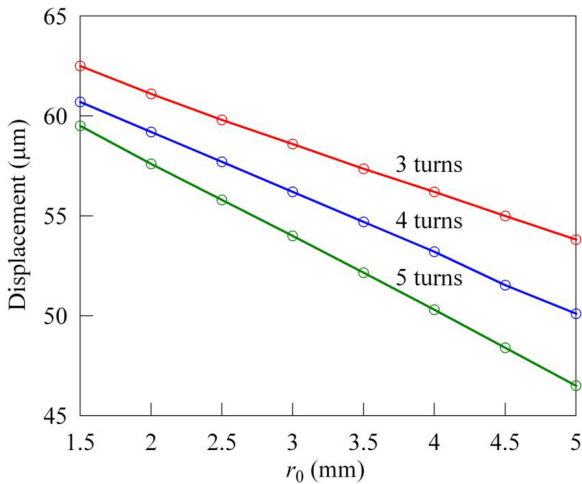


Figure 13. Tangential tip displacement versus the number of turns and the initial radius r_0 .

6. Conclusions

The article presents a GeX hybrid-mixed four-node piezoelectric solid-shell element based on the SaS formulation in which displacements and electric potentials of SaS are utilized as fundamental shell unknowns. The SaS are located at Chebyshev polynomial nodes inside the shell body that improve the behavior of higher-order Lagrange interpolations. To implement the efficient analytical integration throughout the element, the extended ANS method for all components of the strain tensor and electric field is employed. The feature of the proposed GeX solid-shell element is that the element stiffness matrices are evaluated without the use of expensive numerical matrix inversion. The developed solid-shell element exhibits excellent performance in the case of coarse mesh configurations and can be recommended for the 3D stress analysis of piezoelectric shells

of complicated geometry, in particular, for the modeling of spiral actuators.

Declaration of conflicting interests

The author(s) declared no potential conflicts of interest with respect to the research, authorship, and/or publication of this article.

Funding

The author(s) disclosed receipt of the following financial support for the research, authorship, and/or publication of this article: This work was supported by the Russian Science Foundation under Grant No. 18-19-00092.

ORCID iD

GM Kulikov  <https://orcid.org/0000-0002-8243-3461>

References

- Allahverdi M, Danforth SC, Jafari M, et al. (2001) Processing of advanced electroceramic components by fused deposition technique. *Journal of the European Ceramic Society* 21: 1485–1490.
- Bakhvalov NS (1977) *Numerical Methods: Analysis, Algebra, Ordinary Differential Equations*. Moscow: Mir Publishers.
- Bathe KJ and Dvorkin EN (1986) A formulation of general shell elements—the use of mixed interpolation of tensorial components. *International Journal for Numerical Methods in Engineering* 22: 697–722.
- Betsch P and Stein E (1995) An assumed strain approach avoiding artificial thickness straining for a nonlinear 4-node shell element. *Communications in Numerical Methods in Engineering* 11: 899–909.
- Buechter N and Ramm E (1992) Shell theory versus degeneration—a comparison in large rotation finite element analysis. *International Journal for Numerical Methods in Engineering* 34: 39–59.
- Carrera E (2003) Theories and finite elements for multilayered plates and shells: A unified compact formulation with numerical assessment and benchmarking. *Archives of Computational Methods in Engineering* 10: 215–296.
- Carrera E and Valvano S (2017) Analysis of laminated composite structures with embedded piezoelectric sheets by variable kinematic shell elements. *Journal of Intelligent Material Systems and Structures* 28: 2959–2987.
- Carrera E, Brischetto S and Nali P (2011) *Plates and Shells for Smart Structures: Classical and Advanced Theories for Modeling and Analysis*. Chichester: John Wiley & Sons.
- Carrera E, Cinefra M, Petrolo M, et al. (2014) *Finite Element Analysis of Structures through Unified Formulation*. Chichester: John Wiley & Sons.
- Carrera E, Valvano S and Kulikov GM (2018) Electro-mechanical analysis of composite and sandwich multilayered structures by shell elements with node-dependent kinematics. *International Journal of Smart and Nano Materials* 9: 1–33.
- Cheng J, Qian C, Zhao M, et al. (2000) Effects of electric fields of the bending behavior of PZT-5H piezoelectric laminates. *Smart Materials and Structures* 9: 824–831.
- Cinefra M, Carrera E and Valvano S (2015) Variable kinematic shell elements for the analysis of electro-mechanical problems. *Mechanics of Advanced Materials and Structures* 22: 77–106.
- Heinonen E, Juuti J and Leppavuori S (2005) Characterization and modelling of 3D piezoelectric ceramic structures with ATILA software. *Journal of the European Ceramic Society* 25: 2467–2470.
- Heyliger P (1997) A note on the static behavior of simply-supported laminated piezoelectric cylinders. *International Journal of Solids and Structures* 34: 3781–3794.
- Hoja SV and Feng W (1998) *Hybrid Finite Element Method for Stress Analysis of Laminated Composites*. New York: Springer.
- Hughes TJR and Tezduyar TE (1981) Finite elements based upon Mindlin plate theory with particular reference to the four-node bilinear isoparametric element. *Journal of Applied Mechanics* 48: 587–596.
- Klinkel S and Wagner W (2006) A geometrically non-linear piezoelectric solid shell element based on a mixed multi-field variational formulation. *International Journal for Numerical Methods in Engineering* 65: 349–382.
- Klinkel S and Wagner W (2008) A piezoelectric solid shell element based on a mixed variational formulation for geometrically linear and nonlinear applications. *Computers and Structures* 86: 38–46.
- Ko Y, Lee PS and Bathe KJ (2017) A new MITC4 + shell element. *Computers and Structures* 182: 404–418.
- Kpeky F, Abed-Meraim F and Daya EM (2018) New linear and quadratic prismatic piezoelectric solid-shell finite elements. *Applied Mathematics and Computation* 319: 355–368.
- Kulikov GM (2001) Refined global approximation theory of multilayered plates and shells. *Journal of Engineering Mechanics* 127: 119–125.
- Kulikov GM and Carrera E (2008) Finite deformation higher-order shell models and rigid-body motions. *International Journal of Solids and Structures* 45: 3153–3172.
- Kulikov GM and Plotnikova SV (2008) Geometrically exact four-node piezoelectric solid-shell element. *Mechanics of Advanced Materials and Structures* 15: 199–207.
- Kulikov GM and Plotnikova SV (2010) Solution of a coupled problem of thermo-piezoelectricity based on a geometrically exact shell element. *Mechanics of Composite Materials* 46: 349–364.
- Kulikov GM and Plotnikova SV (2011a) Exact geometry piezoelectric solid-shell element based on the 7-parameter model. *Mechanics of Advanced Materials and Structures* 18: 133–146.
- Kulikov GM and Plotnikova SV (2011b) Finite rotation piezoelectric exact geometry solid-shell element with nine degrees of freedom per node. *Computers Materials & Continua* 23: 233–264.
- Kulikov GM and Plotnikova SV (2011c) On the use of a new concept of sampling surfaces in a shell theory. *Advanced Structured Materials* 15: 715–726.
- Kulikov GM and Plotnikova SV (2013) A sampling surfaces method and its application to three-dimensional exact solutions for piezoelectric laminated shells. *International Journal of Solids and Structures* 50: 1930–1943.
- Kulikov GM and Plotnikova SV (2015) The use of 9-parameter shell theory for development of exact geometry 12-node

- quadrilateral piezoelectric laminated solid-shell elements. *Mechanics of Advanced Materials and Structures* 22: 490–502.
- Kulikov GM and Plotnikova SV (2017a) An analytical approach to three-dimensional coupled thermoelectroelastic analysis of functionally graded piezoelectric plates. *Journal of Intelligent Material Systems and Structures* 28: 435–450.
- Kulikov GM and Plotnikova SV (2017b) Benchmark solutions for the free vibration of layered piezoelectric plates based on a variational formulation. *Journal of Intelligent Material Systems and Structures* 28: 2688–2704.
- Kulikov GM, Mamontov AA and Plotnikova SV (2015) Coupled thermoelectroelastic stress analysis of piezoelectric shells. *Composite Structures* 124: 65–76.
- Kulikov GM, Plotnikova SV and Carrera E (2018) Hybrid-mixed solid-shell element for stress analysis of laminated piezoelectric shells through higher-order theories. *Advanced Structured Materials* 81: 45–68.
- Lee S, Goo NS, Park HC, et al. (2003) A nine-node assumed strain shell element for analysis of a coupled electro-mechanical system. *Smart Materials and Structures* 12: 355–362.
- Lee SM, Jun SH, Park CS, et al. (2008) Spiral-shaped piezoelectric actuator fabricated using thermoplastic co-extrusion process. *Sensors and Actuators* 148: 245–249.
- Lentzen S (2009) *Nonlinearly coupled thermopiezoelectric modelling and FE-simulation of smart structures* (Fortschritt-Berichte VDI, Reihe 20, Nr. 419). Düsseldorf: VDI Verlag.
- Li T and Gianchandani YB (2006) A micromachining process for die-scale pattern transfer in ceramics and its application to bulk piezoelectric actuators. *Journal of Microelectromechanical Systems* 15: 605–612.
- MacNeal RH (1982) Derivation of element stiffness matrices by assumed strain distributions. *Nuclear Engineering and Design* 70: 3–12.
- Mohammadi F, Kholkin AL, Jadidian B, et al. (1999) High-displacement spiral piezoelectric actuators. *Applied Physics Letters* 75: 2488–2490.
- Park KC and Stanley GM (1986) A curved C^0 shell element based on assumed natural-coordinate strains. *Journal of Applied Mechanics* 53: 278–290.
- Sze KY and Yao LQ (2000) A hybrid stress ANS solid-shell element and its generalization for smart structure modelling. Part I: Solid-shell element formulation. *International Journal for Numerical Methods in Engineering* 48: 545–564.
- Sze KY, Yao LQ and Yi S (2000) A hybrid stress ANS solid-shell element and its generalization for smart structure modelling. Part II: Smart structure modelling. *International Journal for Numerical Methods in Engineering* 48: 565–582.
- Tan XG and Vu-Quoc L (2005) Optimal solid shell element for large deformable composite structures with piezoelectric layers and active vibration control. *International Journal for Numerical Methods in Engineering* 64: 1981–2013.
- Vidal P, Gallimard L and Polit O (2016) Modeling of piezoelectric plates with variables separation for static analysis. *Smart Materials and Structures* 25: 055043.
- Yao LQ and Sze KY (2009) A hybrid-stress solid-shell element for non-linear analysis of piezoelectric structures. *Science in China Series E Technological Sciences* 52: 575–583.
- Yi S, Ling SF and Ying M (2000) Large deformation finite element analyses of composite structures integrated with piezoelectric sensors and actuators. *Finite Elements in Analysis and Design* 35: 1–15.
- Zheng S, Wang X and Chen W (2004) The formulation of a refined hybrid enhanced assumed strain solid shell element and its application to model smart structures containing distributed piezoelectric sensors/actuators. *Smart Materials and Structures* 13: N43–N50.
- Zienkiewicz OC and Taylor RL (2000) *The Finite Element Method. Volume 1: The Basis*. 5th ed. Oxford: Butterworth Heinemann.
- Zouari W, Assarar M, Meftah K, et al. (2015) Free vibration analysis of homogeneous piezoelectric structures using specific hexahedral elements with rotational DOFs. *Acta Mechanica* 226: 1737–1756.
- Zouari W, Ayad R, Ben Zineb T, et al. (2012) A piezoelectric 3D hexahedral curvilinear finite element based on the space fiber rotation concept. *International Journal for Numerical Methods in Engineering* 90: 87–115.
- Zouari W, Ben Zineb T and Benjeddou A (2009) A FSDT-MITC piezoelectric shell finite element with ferroelectric non-linearity. *Journal of Intelligent Material Systems and Structures* 20: 2055–2075.